Research Square

Preprints are preliminary reports that have not undergone peer review.
They should not be considered conclusive, used to inform clinical practice,
or referenced by the media as validated information.

Physiological and transcriptomic responses of Dendrocalamus latiflorus to salt stress and genome-wide analysis of the WRKY gene family

hang tao
Fujian Agriculture and Forestry University
Lulu Pu
Fujian Agriculture and Forestry University
Rong Xiang
Fujian Agriculture and Forestry University
Cailing Song
Fujian Agriculture and Forestry University
Liguang Chen
Fujian Agriculture and Forestry University
Tianyou He
Fujian Agriculture and Forestry University
Lingyan Chen
Fujian Agriculture and Forestry University
Jundong Rong
Fujian Agriculture and Forestry University
Yushan Zheng
zys1960@163.com

Fujian Agriculture and Forestry University

Research Article

Keywords: Dendrocalamus latiflorus, salt stress, physiological and biochemical responses, transcriptome, WRKY gene family, expression analysis

Posted Date: November 23rd, 2026

DOI: https://doi.org/10.21203/rs.3.rs-11580370/v1

License: This work is licensed under a Creative Commons Attribution 4.0 International License.
Read Full License

Additional Declarations: No competing interests reported.

Physiological and transcriptomic responses of *Dendrocalamus latiflorus* to salt stress and genome-wide analysis of the WRKY gene family

Hang Tao[1], Lulu Pu[1], Rong Xiang[1], Cailing Song[1], Liguang Chen[1], Tianyou He[2], Lingyan Chen[2], Jundong Rong[1*], Yushan Zheng[1*]

[1] College of Forestry, Fujian Agriculture and Forestry University, Fuzhou 350002, China;

2 College of Landscape Architecture and Art, Fujian Agriculture and Forestry University, Fuzhou 350002, China

* Correspondence: Jundong Rong (rongjd@fafu.edu.cn); Yushan Zheng (zys1960@163.com)

Abstract

Background: The physiological and transcriptional responses of *Dendrocalamus latiflorus* to salinity, including the involvement of WRKY factors, remain incompletely understood. We exposed plants to 0%, 0.5%, 1.0% and 1.5% NaCl and combined physiological measurements, RNA sequencing, pathway mapping, qRT-PCR and genome-wide WRKY analysis to identify candidates for functional validation.

Results: Catalase activity reached 2.02 times the control level at 0.5% NaCl. At 1.5% NaCl, malondialdehyde and proline contents reached 1.95 and 2.70 times the control, respectively, while carotenoid content decreased by 15.8%. The three salt treatments yielded 2757, 4424 and 3153 candidate differentially expressed genes at nominal $P < 0.05$ and $|\log_2 FC| > 1$. At false discovery rate < 0.05 and the same fold-change cutoff, 289 genes remained at 1.0% NaCl and none at the other concentrations. Arginine and proline metabolism was enriched in all treatments at nominal $P < 0.05$, with transcriptional responses concentrated on P5CS candidates. Seventeen coordinate-matched WRKY members showed induced, repressed or mixed responses. qRT-PCR and RNA-seq agreed in direction for 29 of 30 gene-treatment comparisons. Genome-wide screening identified 488 candidate WRKY models and 245

A1/B1/C1 representative members, comprising 29 I-like, 166 II-like, 46 III-like and four atypical members. ABRE and W-box cores occurred in 90.16% and 88.11% of evaluable upstream regions, respectively.

Conclusions: *Dendrocalamus latiflorus* showed concentration-dependent physiological and transcriptional responses to salinity. Expression patterns, protein integrity and promoter motifs supported the selection of *DlWRKY004* and the P5CS candidate Dl3AG001551 for functional testing. Binding and regulation have yet to be validated, and the nominal-P candidate sets remain exploratory.

Keywords: *Dendrocalamus latiflorus*; salt stress; physiological and biochemical responses; transcriptome; WRKY gene family; expression analysis.

1. Background

Plants adapt to salt stress through ion transport, osmotic adjustment and the allocation of resources to growth, rather than through a single metabolic pathway. Natural variation and phosphorylation of soybean GmNPF7.5 alter Cl^- uptake while preserving nitrate permeability, indicating that anion transport contributes to differences in salt tolerance [1]. In maize, the SnRK2-HAK module enhances Na^+ exclusion through protein phosphorylation, so salt tolerance also depends on regulation beyond changes in transcript abundance [2]. Reciprocal regulation between the Arabidopsis CBL-CIPK and TOR complexes connects salt adaptation with growth recovery [3]. Understanding these responses requires separate evidence for physiological changes, gene expression and the specific regulatory events involved.

Osmotic adjustment and redox homeostasis connect stress perception with physiological responses. In Arabidopsis root cells, osmotic stimulation induces membrane nanodomains enriched in H_2O_2, indicating that reactive oxygen species (ROS) act as spatially controlled signals [4]. The glutamate-derived proline biosynthesis branch, which begins with Δ^1-pyrroline-5-carboxylate synthase (P5CS), contributes to osmotic adjustment. Silencing cotton

GhP5CS1 increases salt sensitivity, providing functional evidence for the role of this branch in salt tolerance [5]. In tomato, the CRY1a-HY5 module regulates *P5CS1* and *OAT* transcription, promotes proline accumulation and enhances salt tolerance under specific light conditions, suggesting that proline biosynthesis integrates multiple upstream signals [6]. Physiological measurements, transcriptome analysis and pathway mapping can therefore help identify the metabolic processes recruited under salt stress and the transcriptional regulators involved.

WRKY transcription factors regulate salt-responsive gene expression in plants. They contain a WRKY domain and can bind W-box elements in target promoters, but their effects depend on the member and its targets. Arabidopsis *WRKY9* regulates the chloride channel gene *AtCLCf*; salt-induced movement of *AtCLCf* from the Golgi to the plasma membrane contributes to salt adaptation [7]. Rice OsWRKY18 binds the *OsHKT1;5* promoter, connecting WRKY activity with Na^+ transport [8]. In apple, *MdWRKY9* participates in ion homeostasis through *MdNHX1* and *MdSOS2*, and its activity is influenced by JAZ proteins and jasmonate signalling [9]. Maize *ZmWRKY17*, however, negatively affects salt tolerance, illustrating why salt-induced expression alone does not establish a positive role in tolerance [10]. WRKY regulation also extends to osmolyte synthesis: tomato SlWRKY42 directly binds the W-box of the *SlP5CS1* promoter and activates transcription [11]. These findings provide a basis for investigating salt-responsive WRKY genes, while requiring both a clear account of their family membership and structure and independent evidence for their downstream targets.

In bamboo, stress-related transcription factors act through several downstream processes. Moso bamboo *PeHDZ72* influences osmotic adaptation through sugar transport and aquaporin-related targets, and its heterologous expression improved drought resistance in rice [12]. PeABF1 binding to the *PeDHN4* promoter, together with *PeDHN* family responses to ABA, NaCl and PEG, connects hormone signalling with protective gene expression [13]. In

Dendrocalamus latiflorus Munro, DREB10-B and DREB12-C bind the *GA2ox7* promoter, suggesting that distinct transcription factor families contribute to environmental responses through different downstream processes [14]. The *D. latiflorus DlamiR156-DlaSPL60-DlaP5CS1* cascade regulates proline synthesis and confers drought resistance [15]. Less is known about the physiological and transcriptional responses of *D. latiflorus* across salt concentrations. Its salt-responsive WRKY members and their family-wide characteristics have not been systematically analysed.

The polyploid genome of *D. latiflorus* complicates the selection and interpretation of candidate genes. This allohexaploid species has three reference subgenomes, A, B and C, each with two haplotypes [16]. Comparisons of genomes and multi-tissue transcriptomes from 11 bamboo species showed that subgenome dominance depends on lineage and can switch direction in hexaploid lineages [17]. Extensive allele-specific expression in a haplotype-resolved nonaploid bamboo genome further illustrates the need to distinguish haplotype gene models from independent family representatives [18]. In hexaploid oat, natural variation in *AsWRKY49-D2* alters its regulatory relationships and drives functional divergence among homoeologs during the salt response [19]. Analyses of the *D. latiflorus* WRKY family must therefore distinguish haplotype models from independent members. Candidate selection also needs to account for ID correspondence, subgenome background and sequence integrity, which cannot be resolved by ranking expression levels or family numbers alone.

We treated *D. latiflorus* with 0%, 0.5%, 1.0% and 1.5% NaCl to examine how leaf physiology and gene expression change across salt concentrations and which metabolic pathways respond. We also investigated the expression patterns of differentially expressed WRKY members, the composition and structure of the family, and its upstream cis-acting elements. A further aim was to identify compounds whose synthesis might involve salt-responsive WRKY factors and to select WRKY and target gene pairs for experimental testing.

We combined physiological and biochemical assays with RNA-seq differential expression and enrichment analyses, proline pathway mapping and qRT-PCR. Genome-wide WRKY identification was followed by phylogenetic, motif, domain and upstream-sequence analyses. Expression associations and promoter W-box sites were then examined for 17 salt-responsive WRKY genes and five P5CS candidates. Together with a WRKY association network predicted from rice homologous proteins, these analyses guided the selection of a gene pair for priority validation. The expression associations and sequence matches generate hypotheses; they do not establish regulation or a mechanism of salt tolerance.

2. Methods

2.1. Plant materials and salt treatment

In March 2024, healthy, pest-free two-year-old main and lateral branches of *Dendrocalamus latiflorus* Munro with well-developed buds were collected from public land in Yunyang Village, Lianhua Town, Tong'an District, Xiamen, Fujian Province, China. The basal and apical ends were wrapped in water-retaining cotton and plastic film to minimise moisture loss. The branches were promptly transported to a greenhouse at Fujian Agriculture and Forestry University, Fujian Province, China, where they were propagated by cuttings. Cutting propagation and the subsequent salt-treatment experiment were conducted in the same greenhouse.

Uniform one-year-old potted seedlings of *Dendrocalamus latiflorus* Munro were grown in a greenhouse with consistent watering and nutrient management. Air temperature ranged from 14 to 30 °C (mean 25 °C), relative humidity was >78%, and the natural photoperiod was approximately 12 h (about 06:00 to 18:00). All pots were maintained under the same watering, light and temperature conditions to minimise environmental variation. Plants received one of four NaCl treatments: 0% (control, T0), 0.5% (T1), 1.0% (T2) or 1.5% (T3), with three independent biological replicates per treatment. Pots were watered to saturation

with the corresponding NaCl solution every 2 to 3 days to maintain a constant soil salt concentration. After treatment, mature functional leaves were collected, snap-frozen in liquid nitrogen and stored at −80 °C for physiological and biochemical measurements and RNA-seq analysis.

2.2. Determination of physiological and biochemical indices

Carotenoids were extracted with 95% ethanol, and absorbance was measured at 665, 649 and 470 nm. SOD, POD and CAT activities were measured using assay kits from Suzhou Keming. MDA content was determined by the thiobarbituric acid colorimetric method, with absorbance measured at 532, 600 and 450 nm. Proline content was determined by the acid ninhydrin colorimetric method. After colour development, the chromophore was extracted with toluene and absorbance was measured at 520 nm. Proline content (mg g^{-1}) was calculated from a standard curve. POD activity is expressed as 10^3 U g^{-1}. Results are reported as mean ± SD (n = 3). The summary data for Fig. 1 are provided in Additional file 1: Table S2.

2.3. RNA-seq and differential expression analysis

Total RNA was extracted from *D. latiflorus* leaves in each NaCl treatment using a total RNA extraction kit (Thermo Fisher Scientific). After RNA quality control, mRNA was enriched and used to construct cDNA libraries for Illumina sequencing. Adapters and low-quality reads were removed, and clean reads were aligned to the *D. latiflorus* reference genome (24411913 v3) with HISAT2 v2.0.5 [20]. Transcripts were assembled with StringTie v1.3.3b [21]. Gene read counts were obtained with featureCounts v1.5.0-p3 [22], and FPKM values were calculated for preliminary inspection of expression levels. Gene-level expected counts and TPM values were estimated with RSEM [23] for all subsequent analyses. Differential expression was analysed with the edgeR 3.40.2 quasi-likelihood pipeline in R 4.2.3, using RSEM gene-level expected counts without rounding fractional values [24]. Low-

expression genes were filtered with filterByExpr within treatment groups (min.count = 10, min.total.count = 15, large.n = 10, min.prop = 0.7). Library sizes were then recalculated and TMM normalisation was applied. A ~treatment model was fitted with T0 as the reference level. Dispersions were estimated with estimateDisp using robust estimation, and models were fitted with glmQLFit (robust = TRUE, prior.count = 0.125). Each of T1, T2 and T3 was compared with T0 using glmQLFTest (poisson.bound = TRUE). Candidate DEGs were defined as genes with nominal $P < 0.05$ and $|\log_2 FC| > 1$. BH-adjusted FDR values were calculated within each comparison and are reported in full in Additional file 2. Principal component analysis (PCA), with gene-wise centring, and Pearson correlations between samples were calculated from the TMM-normalised $\log_2 CPM$ values (prior.count = 2) of the tested genes.

2.4. Gene expression patterns and functional enrichment analysis

The union of candidate DEGs was standardised by row to Z-scores (ddof = 1) and hierarchically clustered using 1 − Pearson r as the distance metric and average linkage. For GO and KEGG enrichment, the background comprised tested genes with annotations in the relevant database. Terms with at least 10 background members were assessed with a one-sided hypergeometric test. BH adjustment was applied separately within each comparison and annotation database. Twelve KEGG pathways and 22 GO terms were selected for display based on their relevance to stress responses; only terms with raw enrichment $P < 0.05$ are shown. Gene ratio was calculated as the number of candidate genes assigned to a term divided by the total number of annotated candidate genes in the corresponding database. The six differentially expressed WRKY genes with the highest mean TPM were also displayed alongside the sample correlation matrix. Link width was scaled to the square root of each sample's TPM, and link colour indicated differential expression status for the corresponding

treatment. These links show expression patterns and do not represent Mantel tests or regulatory relationships.

2.5. Expression mapping of the proline biosynthesis pathway and salt-responsive WRKY genes

The glutamate-derived proline biosynthesis pathway was reconstructed from KEGG module M00015. P5CS (K12657) and P5CR (K00286) candidates were identified from KO and functional annotations [25]. For each enzyme candidate included in the differential expression test, $\log_2$FC values for T1, T2 and T3 relative to T0 were plotted in a heatmap. Candidates meeting the combined threshold were marked with asterisks. The same expression profiles were shown at both P5CS-catalysed steps because P5CS is a bifunctional enzyme. Conversion of glutamate 5-semialdehyde (GSA) to Δ^1-pyrroline-5-carboxylate (P5C) was labelled as non-enzymatic. The figure also includes WRKY genes with exact coordinate matches that met the selection criteria in at least two comparisons. Dashed lines indicate regulatory hypotheses that have yet to be tested.

2.6. Quantitative real-time PCR (qRT-PCR)

Ten candidate genes associated with salt stress were selected for qRT-PCR based on their transcriptome annotations and expression levels. Primers were designed with NCBI Primer-BLAST [26]; their sequences are listed in Additional file 1: Table S1. Leaf RNA from each NaCl treatment was treated to remove genomic DNA and reverse-transcribed into first-strand cDNA. qRT-PCR used this cDNA as the template and *GAPDH* as the reference gene, with three independent biological replicates per treatment. Target and reference Ct values were paired by sample ID. For each sample, ΔCt was calculated as Ct(target) − Ct(*GAPDH*). The mean ΔCt of the 0% NaCl control for the same gene served as the calibrator. Relative expression was calculated by the $2^{-\Delta\Delta Ct}$ method [27], assuming an amplification factor of 2 for both target and reference genes, and is reported as mean ± SD. Pairwise comparisons were

199 performed on the ΔCt scale using the Games-Howell test (α = 0.05). The direction of each
200 treatment response relative to the control was compared with the corresponding RNA-seq
201 result [28].
202
203 **2.7. Genome-wide identification and phylogenetic analysis of the WRKY family**
204 The *D. latiflorus* reference genome and annotation were obtained from the public
205 Figshare dataset (24411913 v3), which includes two haplotypes for each of the A, B and C
206 subgenomes. WRKY domains were identified with HMMER 3.4 using the PF03106.22
207 model. Candidates were retained when both sequence and domain scores met the gathering
208 (GA) threshold of 21 bits and model coverage was ≥ 0.65 [29]. Models containing the
209 PF00931 domain were recorded separately as NLR-WRKY fusions. A representative set was
210 assembled from the A1, B1 and C1 haplotypes. Members were provisionally classified as I-
211 like, II-like, III-like or Atypical according to WRKY domain number and C-terminal zinc-
212 finger type.
213 One C-terminal WRKY domain was extracted from each protein for phylogenetic analysis.
214 Fragments ≥ 40 aa long with ≤ 10% ambiguous residues (X) were retained and combined with
215 69 *Arabidopsis* and 9 rice reference domains. Sequences were aligned with MAFFT 7.526 (L-
216 INS-i), and columns with ≥ 50% non-gap occupancy were retained [30]. A maximum-
217 likelihood tree was inferred with IQ-TREE 2.4.0. ModelFinder Plus selected the best-fit
218 substitution model according to the Bayesian information criterion (BIC). Branch support was
219 assessed with 1,000 replicates each of SH-aLRT and ultrafast bootstrap (UFBoot), with -bnni
220 enabled and the random seed set to 20261021 [31]. Branches with SH-aLRT ≥ 80 and
221 UFBoot ≥ 95 were considered highly supported. The tree was interpreted as unrooted.

2.8. Conserved motif, domain and promoter cis-acting element analyses

Conserved motifs in the 245 A1/B1/C1 representative proteins were identified with MEME 5.5.9 using the ZOOPS model, a maximum of 10 motifs, motif widths of 6 to 50 aa and a random seed of 20261021 [32]. Domain annotations were obtained from the HMMER results described in Section 2.7. To illustrate structural diversity, proteins were grouped by structural type and subgenome. From each non-empty group, we selected the protein closest to the group's median length; ties were resolved by lexicographic order of gene ID. This procedure selected 11 members for display in the main text, independently of expression level, differential expression, motif composition or cis-acting element results. Results for the entire family are provided in Additional file 2.

For each gene, up to 2,000 bp upstream of the annotated 5′ boundary was extracted according to strand orientation. The sequence was truncated at the nearest neighbouring coding gene or chromosome end. Both strands were scanned locally for exact or IUPAC matches to a fixed-length panel of motifs derived from PlantCARE [33], supplemented with the TTGACC/TTGACT-type W-box core motif. Overlapping and equivalent matches within each category were merged. This scan identified candidate sequences; no statistical enrichment test was performed. Positions were measured relative to the annotated 5′ boundary, set to 0, rather than an experimentally determined transcription start site.

2.9. Prioritisation of candidate WRKY and P5CS pairs

Eighty-five candidate pairs were formed from the 17 WRKY genes described in Section 2.5 and the five P5CS genes. Pearson and Spearman correlations were calculated from $\log_2(\mathrm{TPM} + 1)$ values across the 12 samples. To assess associations after accounting for treatment effects, we subtracted the treatment mean from each sample value and calculated Pearson correlations between the resulting residuals. All $6^4 = 1{,}296$ within-treatment permutations, including the observed arrangement, were enumerated. The two-sided exact P

value was the proportion of permutations with |r| at least as large as the observed value. For each correlation test, P values were adjusted across the 85 pairs using the Benjamini-Hochberg (BH) procedure, with $q < 0.05$ considered significant. Sensitivity was assessed by removing each sample in turn and recalculating treatment means and residuals.

The 2-kb upstream sequences of P5CS candidates were extracted according to strand orientation, and neighbouring gene boundaries were checked. Both strands were scanned for TTGACC and TTGACT, with the coordinates, sequences and orientations of matches recorded. CDS start and end positions, translation consistency and the presence of two catalytic domains were checked for each candidate. Candidates were prioritised for experiments based on confidence in gene identity, protein completeness, expression response and the presence of cis-acting sites that could be tested. This ranking reflects suitability for experimental testing, not the probability of regulation.

2.10. Prediction of WRKY association networks based on rice homologs

Full-length sequences of the 245 representative *D. latiflorus* WRKY proteins were searched against the STRING *japonica* rice protein database (taxon 39947; sequence release 12.0) using DIAMOND 2.2.8 blastp in ultra-sensitive mode, retaining up to 20 hits per query. Hits were required to have E-value $\leq 10^{-10}$, sequence identity $\geq 30\%$ and alignment coverage $\geq 50\%$ of both query and reference protein lengths. Reference proteins also had to meet PF03106 sequence and domain scores ≥ 21 and model coverage $\geq 65\%$. The qualifying hit with the highest bitscore was selected for each query. Mappings were flagged as near-tied when the second-best score was $\geq 95\%$ of the top score. Best hits were not assumed to be one-to-one orthologs.

Reference IDs were verified through the STRING 12.5 API. Functional and physical association networks were then retrieved separately at a combined score ≥ 0.400, with add_nodes = 0 (retrieved 24 October 2026) [34]. For reference-network statistics, *D. latiflorus*

members mapping to the same reference protein were merged into one node. WRKY family members were tested for differential expression after low-expression filtering. The 66 members with nominal $P < 0.05$ and $|\log_2 FC| > 1$ in at least one salt treatment relative to the control were designated salt-responsive candidates. An induced subnetwork was constructed from these candidates, and connected nodes and their associations were displayed in the main text according to homology mapping. Networks for the entire family and the subset of candidates with exact coordinate matches were also provided. Sensitivity was assessed using a stricter mapping subset with identity ≥ 40%, bidirectional coverage ≥ 60% and no near-tied mappings. These networks predict associations from a reference species. They neither establish salt-treatment-specific networks nor demonstrate experimentally measured interactions in *D. latiflorus*.

2.11. Use of generative AI tools

OpenAI ChatGPT/Codex assisted with drafting and editing the text, developing analysis and plotting scripts, and preparing manuscript files. It was not used to generate experimental measurements. The authors remain responsible for the data, analyses, interpretations and submitted text.

3. Results

3.1. Pigments, proline and antioxidant enzymes respond differently to salt concentration

At the highest salt concentration, *D. latiflorus* leaves showed significantly greater membrane lipid peroxidation and lower carotenoid content (Fig. 1a,b). Carotenoid content did not differ significantly between T1 and T0. It reached 5.25 ± 0.52 mg g^{-1} at T2, 22.1% above T0, then fell to 3.62 ± 0.09 mg g^{-1} at T3, 15.8% below T0. MDA content increased from 12.52 ± 1.08 μmol g^{-1} in T0 to 24.47 ± 0.48 μmol g^{-1} in T3, 1.95 times the control value. This increase is consistent with greater damage associated with membrane lipid peroxidation at the highest salt level.

297 Proline content increased steadily with NaCl concentration (Fig. 1c), from 10.07 ± 1.00
298 mg g^{-1} at T0 to 18.11 ± 0.96, 21.03 ± 0.88 and 27.18 ± 0.78 mg g^{-1} at T1, T2 and T3,
299 respectively. These treatment values were 1.80-, 2.09- and 2.70-fold the control value. All
300 four treatments differed significantly from one another ($P < 0.05$).

301 The three antioxidant enzymes showed different responses to increasing salt
302 concentration (Fig. 1d-f). SOD activity fell to 158.58 ± 15.14 U g^{-1} at T1 and partly recovered
303 at T2 and T3, although the means remained below the control. POD activity was lower than
304 the control in all three salt treatments, with no significant differences among the salt
305 treatments. CAT activity peaked at T1, reaching 761.90 ± 45.90 nmol min^{-1} g^{-1}, 2.02 times
306 the control value, and then declined as salinity increased. The distinct responses of these
307 enzymes indicate that changes in a single enzyme do not fully describe the antioxidant
308 response.

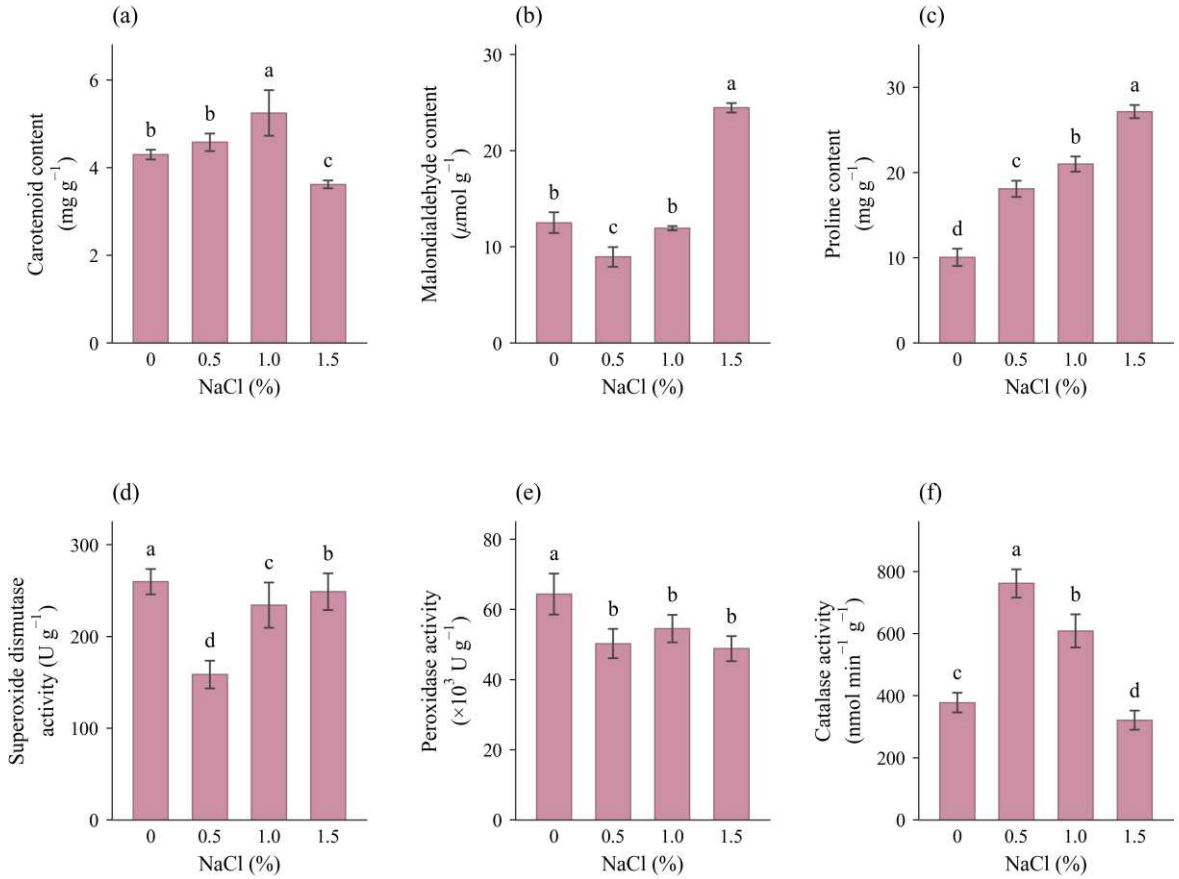


Fig. 1. Physiological responses of *Dendrocalamus latiflorus* leaves to NaCl treatments. (a) Carotenoids; (b) MDA; (c) proline; (d) SOD; (e) POD; (f) CAT. T0, T1, T2 and T3 denote 0%, 0.5%, 1.0% and 1.5% NaCl, respectively. Bars and error bars represent mean ± SD (n = 3). Different lowercase letters indicate significant differences among treatments ($P < 0.05$).

3.2. The transcriptional response is greatest at moderate salinity

After expression filtering, 33,439 gene models were tested for differential expression. Principal component analysis (PCA) showed that PC1 and PC2 explained 30.4% and 20.9% of the expression variance, respectively, accounting for 51.3% together. T2 samples clustered relatively tightly, whereas T0 and T1 samples were more dispersed within their groups (Fig. 2a).

The number of candidate DEGs increased from T1 to T2 and then declined at T3 (Fig. 2b-d). At the combined threshold of nominal $P < 0.05$ and $|\log_2 FC| > 1$, the comparisons of T1, T2 and T3 with T0 yielded 2,757 (1,006 upregulated and 1,751 downregulated), 4,424 (2,247

upregulated and 2,177 downregulated) and 3,153 (951 upregulated and 2,202 downregulated) candidate DEGs, respectively. The three sets contained 6,265 unique candidate DEGs, including 1,338 shared by all three comparisons. T3 had the highest proportion of downregulated candidates, at 69.8% (2,202/3,153). Applying FDR < 0.05 together with the fold-change cutoff retained 289 DEGs in T2 and none in T1 or T3. Enrichment analyses therefore used the candidate sets defined by nominal P.

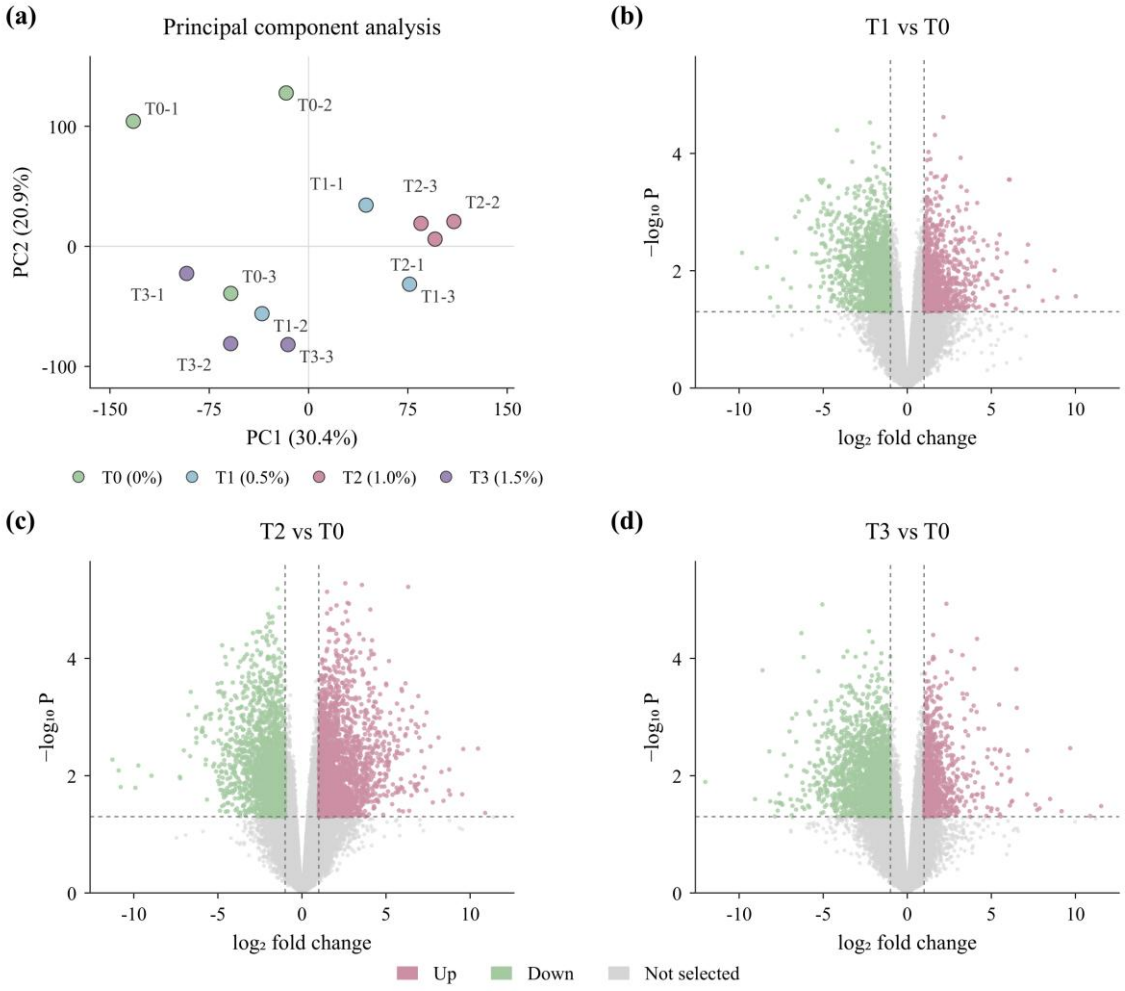


Fig. 2. Transcriptome variation and candidate differentially expressed genes under salt treatment. (a) PCA of TMM-normalised log2CPM values for the 33,439 tested genes; each point represents one biological sample. (b-d) Volcano plots for T1, T2 and T3 relative to T0. Pink and green indicate upregulated and downregulated candidate genes, respectively, and grey indicates genes not selected. Candidates met nominal P < 0.05 and |log2FC| > 1.

3.3. Candidate DEGs are enriched in pathways for osmotic adjustment, signal transduction and secondary metabolism

Hierarchical clustering separated the 6,265 candidate DEGs into distinct expression subgroups across the 12 samples (Fig. 3a).

Arginine and proline metabolism was enriched in all three salt treatments (nominal enrichment $P < 0.05$), suggesting a shared role for osmotic adjustment in the salt response of *D. latiflorus* (Fig. 3b). The pathway contained 16, 23 and 21 DEGs in T1, T2 and T3, with enrichment P values of 4.75×10^{-4}, 8.37×10^{-6} and 5.70×10^{-6}, respectively. Phenylpropanoid biosynthesis, fatty acid elongation and plant-pathogen interaction were also enriched in all three treatments (nominal $P < 0.05$). At T2, plant hormone signal transduction and the MAPK signalling cascade showed strong enrichment, with 118 and 55 DEGs, respectively.

The GO results were consistent with the KEGG analysis (Fig. 3c). The term "proline biosynthetic process" included 12, 13 and 14 candidate genes in T1, T2 and T3, respectively ($P < 0.05$). Enriched terms also covered water transport (aquaporins), transmembrane potassium transport, glycine betaine synthesis and the abscisic acid-activated signalling pathway. These results indicate contributions from osmoprotection, ion transport and signal transduction to the transcriptional response.

The most highly expressed WRKY genes among the candidate DEGs were induced mainly at T2 (Fig. 3d). Ranked by mean TPM across the 12 samples, the top six were *DlWRKY070* (Dl6AG000660), *DlWRKY147* (Dl15AG000613), *DlWRKY206* (Dl27AG000338), *DlWRKY200* (Dl25AG000341), *DlWRKY057* (Dl4AG000337) and *DlWRKY024* (Dl2AG000610). Member numbering follows the genome-wide identification described in Section 2.7 and reported in Section 3.6. *DlWRKY200* showed treatment-specific

expression, whereas the other five members were upregulated at T2 (nominal $P < 0.05$ and $|\log_2FC| > 1$).

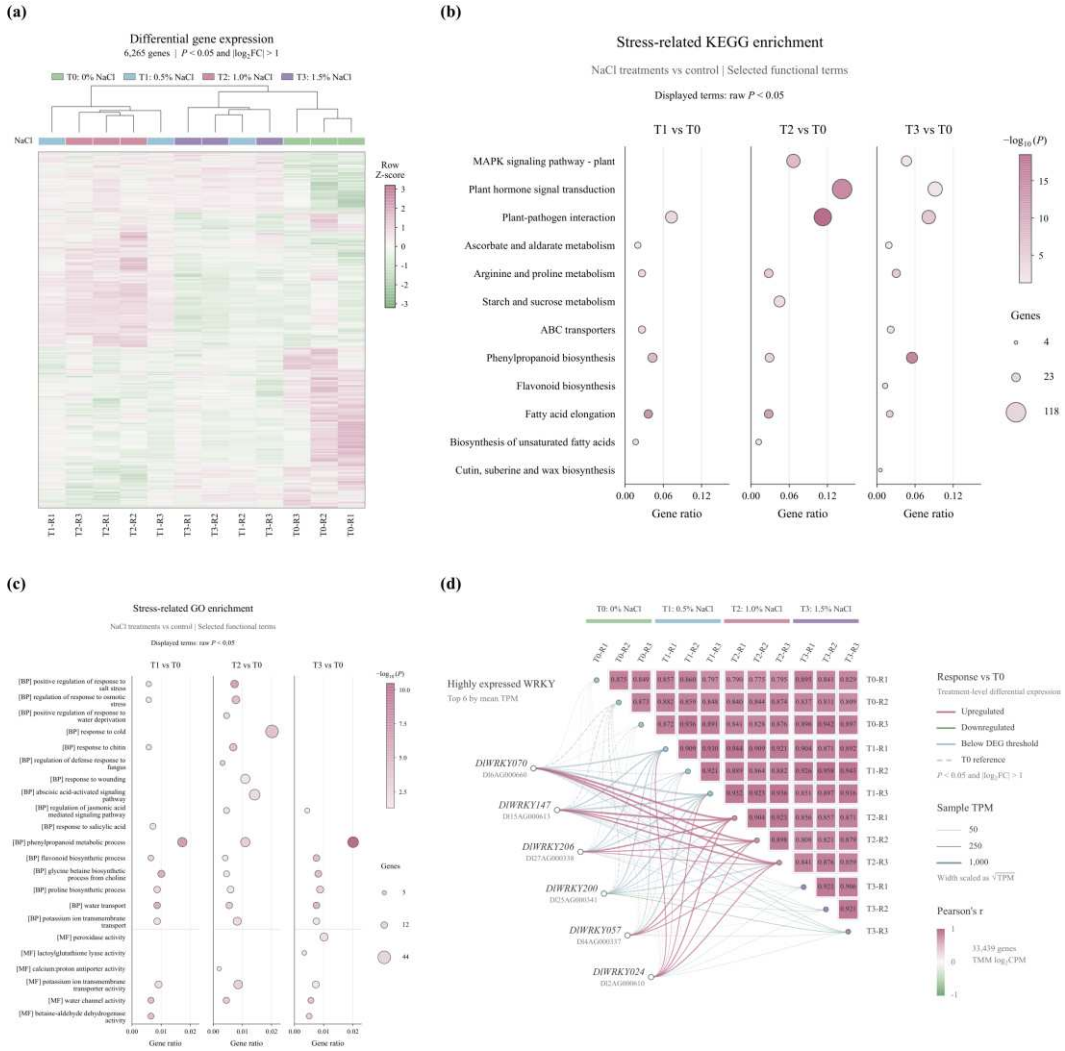


Fig. 3. Expression patterns, functional enrichment and highly expressed WRKY genes. (a) Row Z-score heatmap of the 6,265 candidate genes. (b,c) Representative stress-related KEGG (b) and GO (c) terms with nominal enrichment $P < 0.05$. Dot area represents gene number, and colour represents $-\log_{10}(P)$. (d) Pearson correlations among the 12 samples, shown alongside the six differentially expressed WRKY genes with the highest mean TPM. Line width scales with single-sample √TPM, and line colour indicates differential expression status for each treatment. The lines display expression levels; they do not represent Mantel tests or regulatory relationships.

3.4. Expression of proline biosynthesis genes and salt-responsive WRKY genes

We reconstructed the glutamate-derived proline biosynthesis pathway using KEGG module M00015. Glutamate is converted through L-glutamyl 5-phosphate to L-glutamate 5-semialdehyde (GSA). GSA then spontaneously cyclises to Δ^1-pyrroline-5-carboxylate (P5C), which is reduced to L-proline. The bifunctional enzyme P5CS catalyses the first two reactions, and P5CR catalyses the final reduction; GSA cyclisation to P5C is non-enzymatic (Fig. 4).

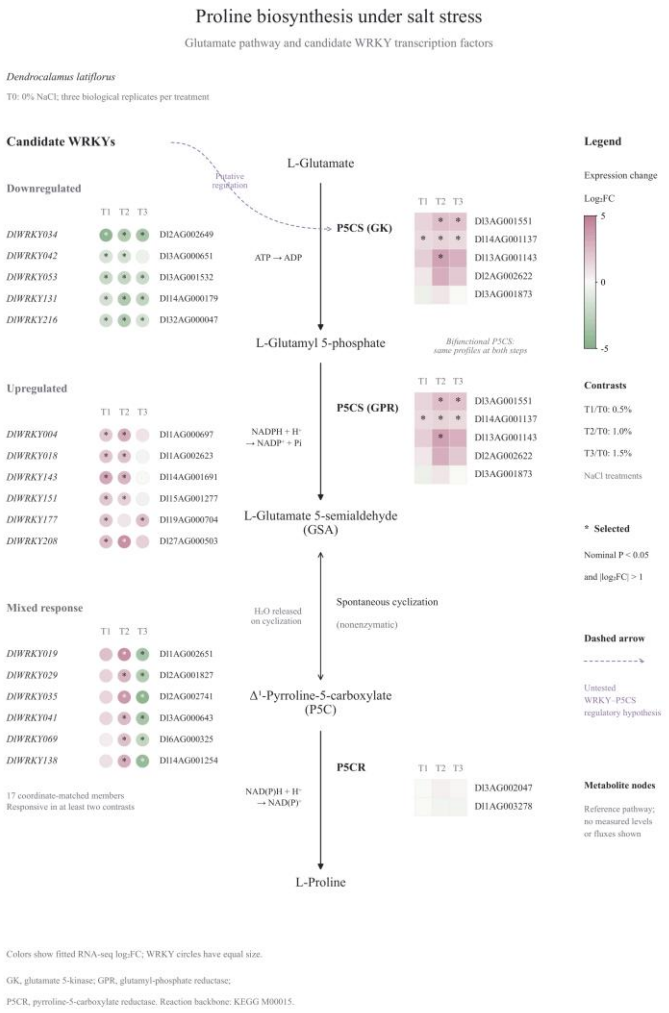


Fig. 4. Glutamate-derived proline biosynthesis and candidate WRKY expression under salt treatment. Heatmaps and equal-sized dots show $\log_2$FC for T1, T2 and T3 relative to T0; asterisks indicate nominal $P < 0.05$ and $|\log_2 FC| > 1$. P5CS is bifunctional and catalyses the first two reactions, so both heatmaps show the same genes. Conversion between GSA and P5C is non-enzymatic. Dashed lines indicate the hypothesised regulation of P5CS by WRKY proteins, which remains untested. Metabolite nodes do not represent measured abundances.

Transcriptional responses in this pathway were concentrated in P5CS. Functional annotation identified 13 P5CS and 2 P5CR candidate gene models; 5 P5CS and 2 P5CR models passed expression filtering and were tested for differential expression. Dl14AG001137 was upregulated in T1, T2 and T3, with $\log_2$FC values of 1.125, 1.301 and 1.076, respectively (nominal $P < 0.05$). Dl3AG001551 was upregulated in T2 and T3 ($\log_2$FC

388 = 2.102 and 1.882, respectively), and Dl13AG001143 was upregulated only in T2 (log_2FC =
389 3.098). The other two P5CS candidates did not meet the significance threshold. Both P5CR
390 genes, Dl3AG002047 and Dl1AG003278, showed only small transcriptional changes, and
391 neither met the combined threshold.

392 The 17 WRKY genes with exact chromosomal coordinates that met the selection criteria
393 in at least two comparisons showed three expression patterns (Fig. 4). *DlWRKY004*,
394 *DlWRKY018*, *DlWRKY143*, *DlWRKY151*, *DlWRKY177* and *DlWRKY208* formed the
395 upregulated group. *DlWRKY034*, *DlWRKY042*, *DlWRKY053*, *DlWRKY131* and *DlWRKY216*
396 were consistently downregulated. *DlWRKY019*, *DlWRKY029*, *DlWRKY035*, *DlWRKY041*,
397 *DlWRKY069* and *DlWRKY138* showed mixed responses.

398 **3.5. Expression changes measured by qRT-PCR largely agree with RNA-seq**

399 qRT-PCR analysis of 10 candidate genes showed different responses to salt
400 concentration (Fig. 5). Of the two non-WRKY targets, *BGAL2-like* (Dl3AG000481) declined
401 progressively as salinity increased, whereas *MPT3-like* (Dl16AG000455) had higher
402 expression at T1 and T2 than at T0 and T3 (Fig. 5a,b). Among the WRKY targets (Fig. 5c-h),
403 *DlWRKY200* reached 12.66 ± 0.83 times the control level at T1, then declined at higher
404 salinity. *DlWRKY004* and *DlWRKY208* both peaked at T2, reaching 6.62 ± 0.75 and 12.67 ±
405 1.48 times the control level, respectively. *DlWRKY019* also peaked at T2 (13.71 ± 1.65-fold)
406 but fell to 0.26-fold at T3. *DlWRKY216* and *DlWRKY053* were significantly repressed in all
407 salt treatments, with expression at T2 falling to 0.16- and 0.25-fold the control level,
408 respectively.

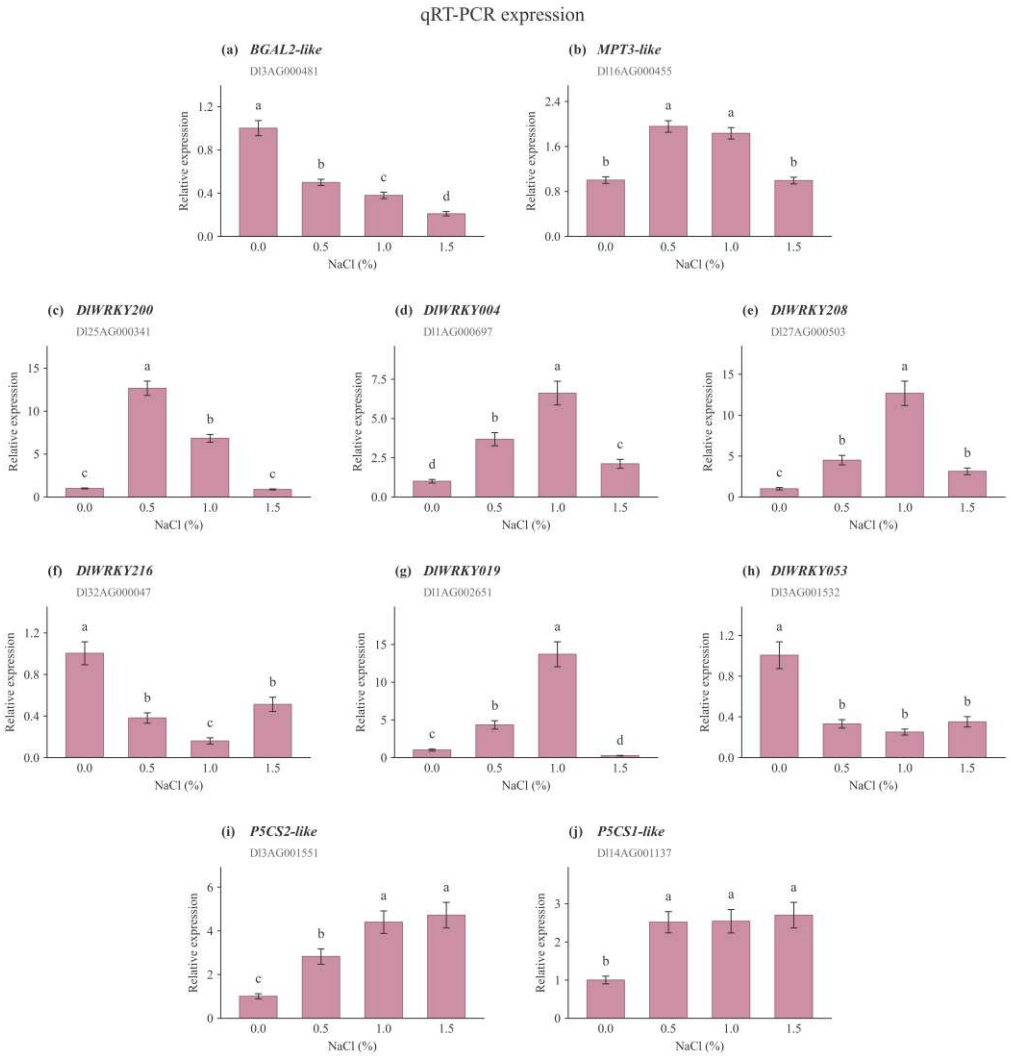


Fig. 5. Relative expression of ten candidate genes under NaCl treatments measured by qRT-PCR. *GAPDH* served as the reference gene, and relative expression was calculated using the $2^{-\Delta\Delta Ct}$ method. Bars and error bars represent mean ± SD of three biological replicates. Treatments sharing no common letter differ significantly (Games-Howell test on ΔCt values, $\alpha = 0.05$). Gene labels follow the functional annotations and primer records. Primer sequences and target identifiers are listed in Additional file 1: Table S1.

Both P5CS candidates were consistently induced by salt treatment (Fig. 5i,j). Dl3AG001551 expression reached 2.82-, 4.40- and 4.72-fold the control level at T1, T2 and T3, respectively. Dl14AG001137 was significantly upregulated in all three salt treatments, with expression approximately 2.51- to 2.70-fold the control level.

qRT-PCR and RNA-seq showed the same direction of expression change in 29 of the 30 gene × treatment combinations (96.7%). The only disagreement was for Dl16AG000455 (*MPT3-like*) in T3 relative to T0: qRT-PCR $\log_2$FC was −0.010, whereas RNA-seq $\log_2$FC was 0.062. Neither estimate was statistically significant.

3.6. Identification, structural classification and phylogeny of the *D. latiflorus* WRKY family

We identified the WRKY family across the *D. latiflorus* genome to establish the family membership and structural features of the salt-responsive genes. Screening 135,231 annotated proteins from all haplotypes identified 490 gene models containing a WRKY domain. Two were NB-ARC-WRKY fusion models and were set aside, leaving 488 candidate WRKY transcription factor models. These models span two haplotype sets, so family analyses used the A1, B1 and C1 representative sets, comprising 83, 85 and 77 members, respectively (245 in total). The representative set contained 29 I-like, 166 II-like, 46 III-like and 4 Atypical members.

Of the 245 representative members, 238 had C-terminal domains that met the criteria for phylogenetic analysis. Together with 69 Arabidopsis and 9 rice reference sequences, they formed a maximum-likelihood tree with 316 tips (Fig. 6). The seven remaining short fragments were retained in the family catalogue. Trimming reduced the initial 80-column alignment to 59 columns, including 49 parsimony-informative sites, and Q.plant+R5 was selected as the best-fit model. The *D. latiflorus* sequences in the tree came from 81, 84 and 73 genes in subgenomes A, B and C, respectively. Among the 302 branches with two support values, 55 met both SH-aLRT ≥ 80 and UFBoot ≥ 95.

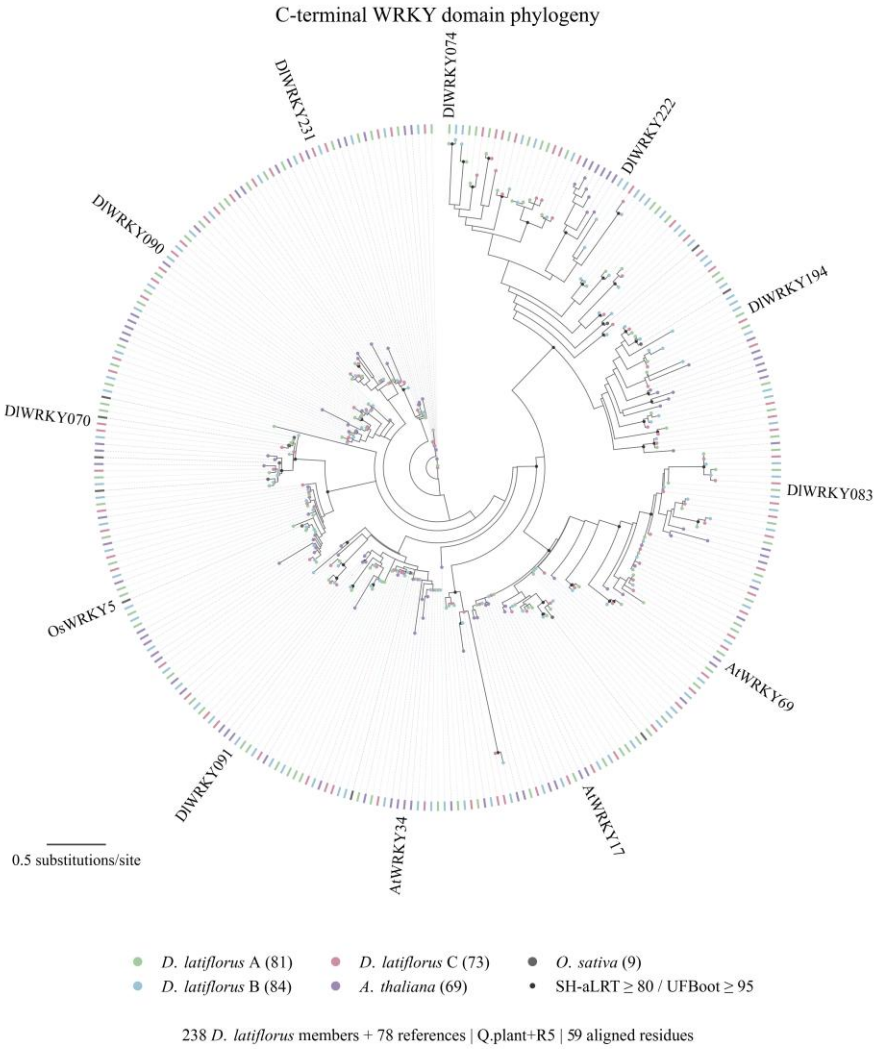


Fig. 6. Phylogeny of representative *Dendrocalamus latiflorus* WRKY C-terminal domains. The maximum-likelihood tree was constructed in IQ-TREE under the Q.plant+R5 model using a 59-column alignment of 238 *Dendrocalamus latiflorus*, 69 Arabidopsis and 9 rice WRKY domains. Colours distinguish subgenomes or reference species. Black dots mark branches with SH-aLRT ≥ 80 and UFBoot ≥ 95 (1,000 replicates each). The scale bar represents substitutions per site. The tree should be interpreted as unrooted.

3.7. Conserved motifs, domains and promoter cis-acting elements of the WRKY family

The representative WRKY members shared a conserved motif centred on WRKYGQK. Structural types differed mainly in domain number and in motifs outside the domains (Fig. 7a,b). Ten conserved motifs, ranging from 11 to 50 aa and comprising 925 sites in total, were identified in the 245 representative proteins. M01, M02 and M03 occurred in 231, 213 and

241 proteins, respectively; the M01 consensus contained the WRKYGQK core. An independent search identified 275 WRKY domains that passed the threshold across the 245 members.

The 11 representatives in Fig. 7 were selected by stratifying members according to structural type and subgenome. The I-like representatives were *DlWRKY235*, *DlWRKY196* and *DlWRKY148*; the II-like representatives were *DlWRKY100*, *DlWRKY108* and *DlWRKY109*; and the III-like representatives were *DlWRKY122*, *DlWRKY133* and *DlWRKY185*. Each type included members from subgenomes A, B and C. The Atypical representatives were *DlWRKY121* from subgenome A and *DlWRKY160* from subgenome B; the subgenome C representative set had no Atypical member. All three I-like representatives carried two WRKY domains, whereas the other eight each carried one. II-like and III-like representatives shared M01, M02 and M03 but differed in motifs outside the domains. Together, the 11 representatives contained 9 of the 10 motifs. Comparison with the expression data showed that *DlWRKY148*, *DlWRKY109* and *DlWRKY122* were upregulated in T2 relative to T0, while *DlWRKY108* was downregulated in T3 relative to T0. All four met nominal $P < 0.05$ and $|\log_2 FC| > 1$, but none met FDR < 0.05. The other five evaluable representatives were not selected. The two Atypical representatives were removed by expression filtering and were therefore not tested. None of these 11 members was among the 10 qRT-PCR targets.

ABRE and the W-box core motif were the most common candidate cis-acting elements in WRKY upstream regions (Fig. 7c). Of the 245 representative members, 244 had an evaluable upstream region; one was recorded as NA because it overlapped a neighbouring gene. ABRE and the W-box core motif occurred in 220 (90.16%) and 215 (88.11%) of the evaluable regions, respectively. CGTCA/TGACG, ARE, MBS, DRE and LTR occurred in 197, 195, 128, 116 and 115 regions, respectively. Element classes and positions varied among

the 11 displayed representatives. Only 30 bp of the upstream region of *DlWRKY121* could be scanned.

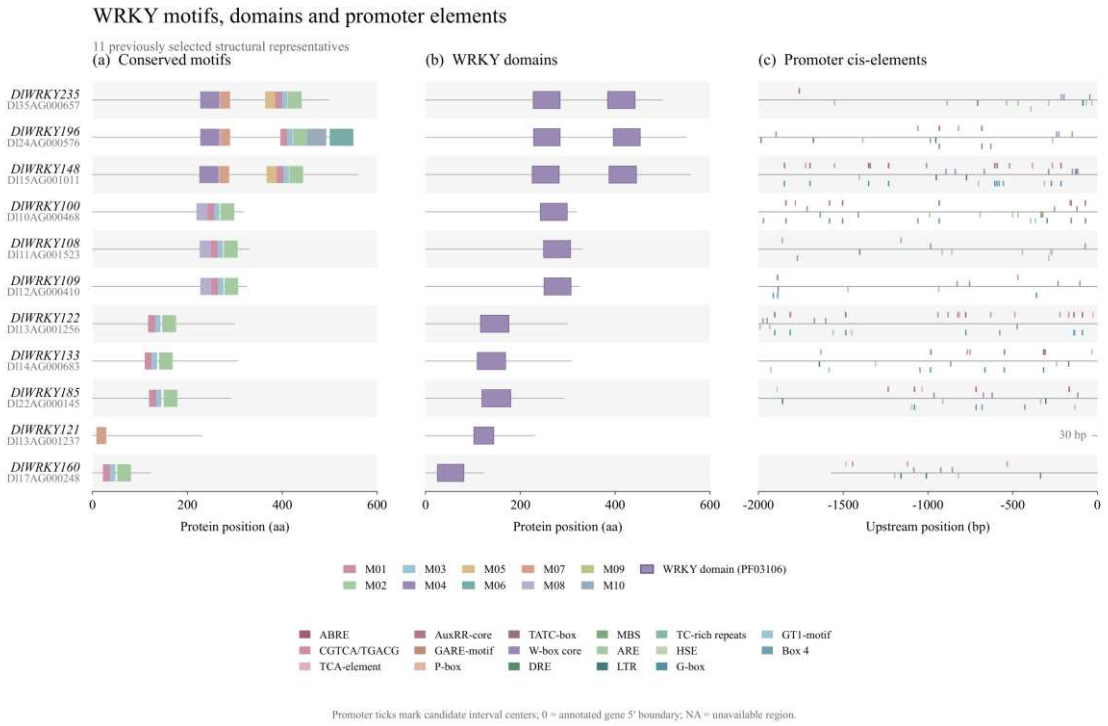


Fig. 7. Conserved motifs, domains and upstream cis-acting elements of representative WRKY members. (a) MEME motifs. (b) PF03106 domains. (c) Candidate cis-acting elements in regions extending up to 2 kb upstream of the gene 5′ boundary, truncated at neighbouring genes. The 11 members were stratified by structural type and subgenome; the protein closest in length to the median of each stratum was selected. This selection was independent of the salt-response results. Family-wide results are provided in Additional file 2. Only 30 bp could be scanned for *DlWRKY121*, so a lack of hits does not imply that regulatory elements are absent.

3.8. Selection and prioritisation of candidate WRKY and P5CS pairs

After accounting for shared treatment effects, no WRKY and P5CS pair showed significant co-expression. None of the 85 pairs formed by 17 WRKY and 5 P5CS candidates met the 0.05 threshold in the within-treatment permutation test after BH adjustment. For *DlWRKY208* and Dl3AG001551, the raw Pearson r was 0.694 and Spearman ρ was 0.692. Subtracting treatment means gave a residual r of 0.590, but the permutation P was 0.371 and

the result was sensitive to individual samples. For *DlWRKY004* and Dl3AG001551, the raw Pearson r was 0.440 and the within-treatment residual r was only 0.025.

Of the five P5CS candidates, Dl3AG001551 had the most complete gene structure and an upstream W-box site suitable for testing. Its 2,151 bp CDS has intact start and stop codons and encodes a 716-aa protein that matches the reference protein. Both domains expected for bifunctional P5CS were present. The 2 kb upstream region contained two TTGACT core motifs, at −1665 to −1660 bp and −1633 to −1628 bp relative to the annotated 5′ boundary. No TTGACC or TTGACT core motif was found upstream of Dl14AG001137, whose correspondence with the transcriptome ID depends on a sorting rule. Dl3AG001873 was annotated as P5CS, but its predicted protein was only 319 aa, with no evidence of both catalytic domains.

Exact ID correspondence, the WRKY domain, the T2 expression response and experimental tractability led us to prioritise *DlWRKY004* (Dl1AG000697) and Dl3AG001551 for validation. *DlWRKY208* (Dl27AG000503) was retained as an alternative transcription factor. *DlWRKY004* had an FDR of 0.0479 in T2/T0. Dl3AG001551 met nominal $P < 0.05$ and $|\log_2 FC| > 1$ in both T2/T0 and T3/T0, although its FDR was ≥ 0.05 in both comparisons. Full pairwise results, promoter sequences and hit coordinates are provided in Additional file 2.

3.9. Predicted associations among salt-responsive WRKY genes based on rice homologs

Of the 245 representative *D. latiflorus* WRKY members, 206 passed the alignment and reference WRKY-domain filters and mapped to 68 rice reference nodes. At a score threshold of 0.400, the family-wide network contained 115 predicted functional associations and 20 predicted physical associations (Additional file 2, network tables). Of the 66 salt-responsive candidates, 59 mapped to 32 reference nodes, while 7 failed to meet the mapping criteria. Their functional association network contained 30 edges, 22 connected nodes and 10 isolated

519 nodes. Fig. 8 displays each of the 39 *D. latiflorus* WRKY genes mapped to the 22 connected
520 reference nodes. Homology mapping expanded the 30 reference associations into 110
521 candidate links.

522 In the network of merged rice reference groups, the group containing *DlWRKY057*,
523 *DlWRKY063* and *DlWRKY070*, which mapped to rice WRKY71, had the highest degree (8). It
524 was followed by *DlWRKY207*, mapped to WRKY76, with a degree of 7. The
525 *DlWRKY019*/*DlWRKY035*/*DlWRKY052* group, mapped to WRKY24, and the group
526 containing *DlWRKY216* each had a degree of 6. The physical-association subnetwork
527 contained 5 predicted edges among 7 nodes. Four edges had database-channel scores, and one
528 was supported only by a text-mining score; all five had an experimental-channel score of 0.

529 Network structure depended on both the score threshold and the mapping criteria. Raising the
530 functional-association threshold to 0.700 left only 5 edges in the salt-responsive subnetwork.
531 Excluding near-tied mappings reduced the subset to 53 candidates mapped to 28 reference
532 nodes, with 20 predicted functional edges and 3 predicted physical edges. Among the 17
533 exact-coordinate candidates in Fig. 4, 14 mapped to 10 reference nodes, with only 3 predicted
534 functional edges and 1 predicted physical edge. Among the 11 structural representatives in
535 Fig. 7, 10 mapped to 7 reference nodes, but no edge between them reached the threshold. The
536 reference group containing *DlWRKY004* was isolated in the salt-responsive subnetwork. This
537 analysis queried only WRKY reference proteins and did not include P5CS.

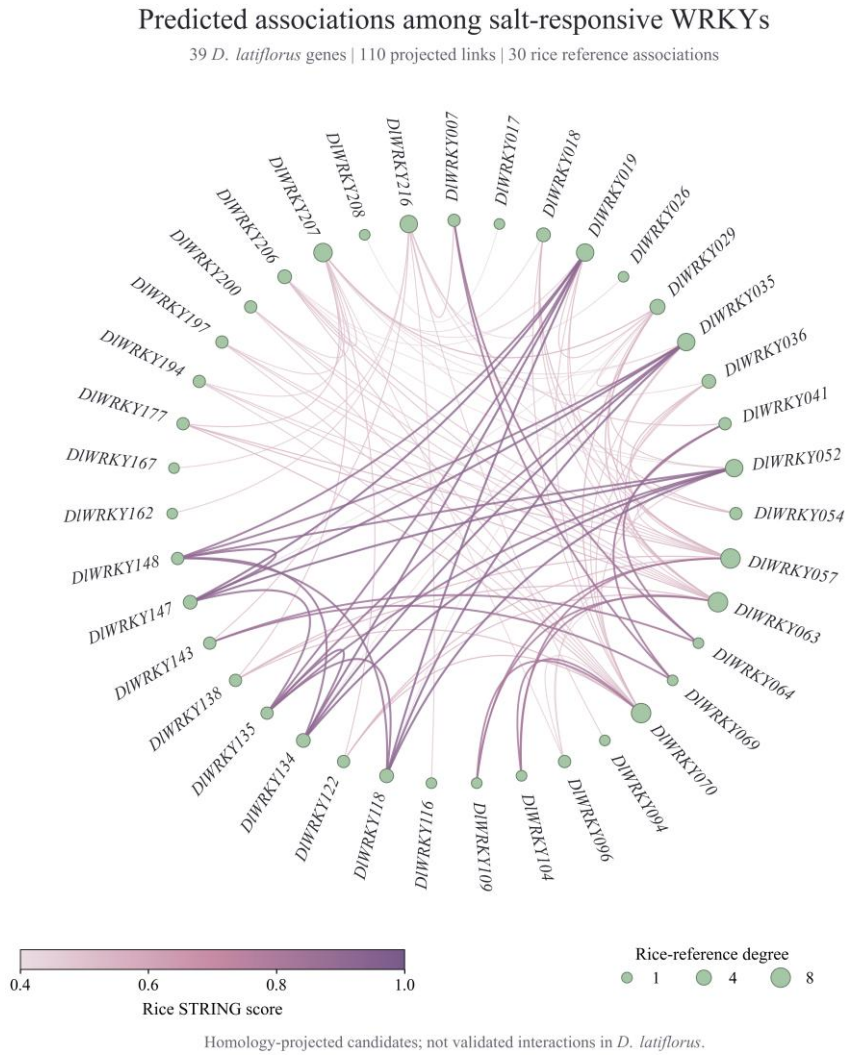


Fig. 8. Predicted associations among salt-responsive *Dendrocalamus latiflorus* WRKY genes mapped to rice homologs. Each of the 39 dots represents one *D. latiflorus* WRKY gene; dot size indicates the degree of its rice reference node. Link colour and width represent the reference STRING score (≥ 0.400). The 110 candidate links were projected from 30 reference associations by homology mapping. No links were added between members of the same reference group. The 39 genes map to 22 connected reference nodes; in total, 59 salt-responsive members mapped to 32 reference nodes. These predictions are based on homology and do not establish direct interactions in *D. latiflorus*.

4. Discussion

4.1. Physiological and biochemical responses of *D. latiflorus* to salt stress

Physiological responses in *D. latiflorus* did not increase uniformly with NaCl concentration. Catalase (CAT) activity increased at low salinity and carotenoid content

peaked at moderate salinity, whereas the highest salt concentration increased membrane lipid peroxidation and reduced carotenoid content (Fig. 1). Proline followed a different pattern, rising steadily to 1.80-, 2.09- and 2.70-fold the control level at T1, T2 and T3, respectively. These differences indicate distinct responses of the physiological processes to increasing salt concentration. Under high salinity, the accumulation of compounds involved in osmotic adjustment occurred alongside damage associated with membrane lipid peroxidation.

Superoxide dismutase (SOD), peroxidase (POD) and CAT responded differently (Fig. 1d-f), suggesting that antioxidant capacity in *D. latiflorus* may be regulated through transcription, protein abundance and enzyme activity. At T1, CAT activity increased while SOD and POD activities fell below control levels. A change in one enzyme therefore does not describe the response of the entire antioxidant system. Studies in other species suggest possible explanations for these differences. In Arabidopsis, CRCK3 phosphorylates CAT2, increasing its activity and reducing ROS accumulation under salt treatment [35]. IBR5 affects both CAT2 activity and phosphorylation, but CAT2 overexpression only partially rescues the salt-sensitive phenotype of *ibr5*, suggesting that other factors also contribute [36]. In rice, STBR1 interacts with and stabilises CATA, promoting H_2O_2 scavenging and defence under saline-alkaline stress [37]. Because catalase activity is also controlled at the protein level, the differences in CAT activity observed across salt concentrations here cannot be attributed directly to the expression of a particular transcription factor.

The increase in malondialdehyde (MDA) under high salinity probably reflects several processes acting together. In Arabidopsis *CAX3* genetic materials, salt tolerance was associated with Ca^{2+} homeostasis, Na^{+} accumulation and antioxidant responses, showing that different upstream processes can produce similar signs of membrane damage [38]. Our measurements indicate increased damage associated with membrane lipid peroxidation at high salinity, together with differing responses of antioxidant enzymes and pigments.

575 Measurements of ions and ROS are needed to establish the causal relationships among
576 membrane damage, ion regulation and ROS scavenging.

577 Proline increased from 10.07 ± 1.00 mg g^{-1} in the control to 27.18 ± 0.78 mg g^{-1} at T3.
578 This change provides direct evidence of a metabolic response to salt in *D. latiflorus* and a
579 physiological context for the *P5CS* expression results. MDA nevertheless remained markedly
580 elevated at T3, so the increase in proline alone does not demonstrate improved salt tolerance.
581 Growth, survival, ion content and ROS levels were not measured concurrently, and the
582 physiological and RNA-seq samples were not established as matched pairs. The data therefore
583 describe responses at the treatment level, without resolving their causal order or individual
584 contributions to salt tolerance.

585 **4.2. Transcriptomic responses of *D. latiflorus* to salt stress**

586 The number of candidate DEGs was greatest at T2, whereas down-regulated genes
587 predominated at T3 (Fig. 2). Salt concentration may therefore change the balance among
588 response processes rather than simply increase the strength of one transcriptional programme.
589 At moderate salinity, enrichment included hormone signalling, the MAPK cascade, water and
590 potassium transport, and osmoprotection (Fig. 3b,c), suggesting contributions from signalling,
591 transport and metabolism. These processes are also regulated beyond transcription. A study of
592 the phosphoproteome and enzyme activities in wolfberry (*Lycium*) found that protein
593 phosphorylation regulated glycolysis and signal transduction under salt treatment [39]. In
594 maize, knockout of *ZmSWEET15a* and *ZmSWEET15b* increased salt sensitivity,
595 demonstrating a role for sugar transport in salt adaptation that is distinct from glycolytic
596 reactions [40]. Responses of the *SbSWEET13* and *SbSUT6* promoters to ABA and MeJA in
597 sorghum further indicate that sugar allocation under salinity depends on genotype and
598 signalling context [41]. The enrichment of both transport and metabolic terms is consistent
599 with several processes responding in parallel; it does not establish a continuous metabolic

chain. Enrichment also identifies processes associated with the response without demonstrating their activation. Similarly, the higher proportion of down-regulated genes at T3 describes the selected gene set and does not establish a global decrease in transcript abundance.

Phenylpropanoid biosynthesis and fatty acid elongation were enriched in all three treatments, suggesting that changes in secondary metabolism and membrane lipids may contribute to adaptation alongside proline metabolism. In alfalfa, the complex formed by MsMYB206, MsMYB450 and MsHY5 connects circadian regulation and flavonoid biosynthesis with salt tolerance [42]. MsEOBI binds and activates the *MsPAL1* promoter, providing an example of direct transcriptional control of the enzyme that initiates phenylpropanoid biosynthesis [43]. Fatty acid desaturase genes in moso bamboo also respond to abiotic stresses and hormones, supporting a role for membrane lipid metabolism in bamboo responses to the environment [44]. These studies provide context for the simultaneous enrichment of phenylpropanoid, fatty acid and signalling terms. Whether the same regulatory relationships and metabolite changes occur in *D. latiflorus* remains unknown.

Within the proline pathway, some *P5CS* candidates responded to salt (Fig. 4; Fig. 5i,j), whereas *P5CR* did not meet the combined threshold (Fig. 4). The detected transcriptional response was therefore concentrated in candidates encoding the enzyme that initiates the pathway. *P5CS* induction and the rise in proline content (Fig. 1c) corresponded at the treatment level, although their responses need not follow a strict one-to-one relationship with salt concentration. The two *P5CS* heatmaps in Fig. 4 show the same genes because the bifunctional enzyme catalyses both initial reactions; they are not independent evidence. *P5CR* falling below the threshold also does not establish that its reaction stopped or that *P5CS* was rate-limiting. In a salt-treatment time series in broccoli, *P5CS* activation and PDH1 suppression accompanied proline accumulation, emphasising the contribution of both

synthesis and degradation to the final proline pool [45]. Exogenous ascorbic acid improved salt tolerance in tomato while reducing excess proline, showing that high proline levels do not invariably indicate greater tolerance [46]. In soybean, exogenous proline reduced ion imbalance and oxidative damage and affected both the glutamate and ornithine pathways, supporting a protective effect under those conditions [47]. Our results show that proline accumulation coincided with expression changes in biosynthetic genes. They do not assign that accumulation to a particular *P5CS* copy, quantify biosynthetic flux or establish its contribution to salt tolerance.

The experimental design and statistical power limit these transcriptomic interpretations. Leaves were collected at one time point with three biological replicates per treatment. T0 and T1 showed some variation among replicates, and no genes met the combined FDR-adjusted threshold at T1 or T3. Gene sets selected using nominal P values are therefore exploratory. Agreement in the direction of expression change between qRT-PCR and RNA-seq applies to the listed targets and does not independently validate the whole transcriptome. Target identity, amplification efficiency and reference-gene stability also require stronger evidence. Sampling across time and including roots, together with concurrent measurements of P5CS activity, proline degradation-related gene expression and growth, would help separate short-term transcriptional responses from metabolite accumulation and salt-tolerance performance.

4.3. WRKY expression under salt stress, family structure and candidate regulatory relationships

4.3.1. Expression responses and functional candidates among WRKY members

The salt-stress transcriptome identified WRKY members as candidate regulators of the response in *D. latiflorus*. Their expression direction does not necessarily predict the direction of their transcriptional effect or their contribution to salt tolerance. The up-regulated, down-regulated and mixed-response groups therefore describe expression patterns, not whether the

proteins act as activators or repressors. ZmWRKY87 promotes salt tolerance by binding to and repressing *ZmPP2C4* transcription, illustrating how repression can have a beneficial effect [48]. WRKY targets also have diverse functions. ZmWRKY107 binds the *ZmPOD52* promoter and modulates antioxidant activity [49]. Arabidopsis WRKY45 binds a W-box in the *RD29A* promoter and directly activates transcription [50]. Persistently down-regulated members such as *DlWRKY216* and *DlWRKY053* thus remain relevant candidates for functional analysis.

WRKY functions vary with tissue, developmental stage and stress conditions, which also limits the scope of our expression classification. In Chinese cabbage (pak choi), the cascade involving BcWRKY25 and BcWRKY33A promotes root elongation and root hair formation under salt conditions through BcLRP1 and BcCOW1 [51]. In alfalfa, MsWRKY75 inhibits seed germination under salt stress through an ABI5-related ABA pathway [52]. Rice OsWRKY12 connects drought responses with secondary cell wall formation through different downstream transcription factors [53]. Our data came from leaves collected at a single time point, so the expression groups apply to that tissue and those treatments. Strong induction of *DlWRKY200* at low salinity, for example, does not identify it as an early responder or establish its function across the whole plant or over time.

WRKY proteins could regulate *P5CS* either by binding its promoter directly or through other transcription factors. In wheat, TaWRKY33 activates *TaERF1-A* during drought, which then regulates *TaP5CS2* and proline synthesis [54]. Other WRKY proteins act through different metabolic pathways. The tomato SlWRKY42 and SlMYC2 module contributes to saline-alkaline tolerance through spermidine synthesis and ion homeostasis [55]. SlWRKY80 regulates *SlSPDS2* and *SlNHX4*, connecting polyamine metabolism with Na^+/K^+ homeostasis under combined saline-alkaline stress [56]. Maize ZmWRKY30 contributes to drought tolerance through inositol and ROS homeostasis [57]. In peony, the PoVQ11 and PoWRKY69

module participates in drought responses through fructose accumulation [58]. *P5CS* was prioritised here because of the combined evidence from pathway enrichment, completeness of the enzyme candidate and expression response. This choice does not imply that proline mediates the effects of every salt-responsive WRKY member.

4.3.2. Phylogenetic and structural features in a polyploid background

Our family analysis distinguished haplotype gene models from individual members. A comparison of bamboo DREB1 genes associated family expansion with polyploidisation and local duplication, while heterologous expression of *PeDREB1A3* tested cold and drought tolerance in one member [59]. An analysis of sugar transporters across 14 bamboo genomes found that whole-genome duplication, subsequent gene loss and subgenome expression divergence shaped family composition [60]. We accordingly reported all-haplotype candidate models, representative members and members retained in the tree separately, avoiding an interpretation of allelic model counts as family expansion. The WRKY tree retained few alignment sites and had limited support for many branches. It can assist family placement, but cannot reliably reconstruct duplication history or establish divergence associated with salt adaptation.

Motif and domain analyses add structural context to the phylogeny. All three I-like representatives in Fig. 7 contain two WRKY domains, while the remaining eight representatives each contain one. The II-like and III-like representatives share the M01-M03 combination but differ in motifs outside the WRKY domain. This pattern is consistent with a conserved WRKY sequence core and variation in the surrounding regions that warrants further comparison. Motif and domain analyses assess structural conservation and completeness, while expression analysis identifies members that respond to salt. Structural similarities or motif differences alone, however, do not establish a role in salt tolerance.

Homoeologs can differ in their stress responses because of regulation at several levels. Wheat HebQTL analysis showed that regulation within subgenomes and compensatory expression between copies can both contribute to unequal homoeolog expression [61]. Transposable elements connect variation in neighbouring sequences with expression and functional differences between homologous genes, showing that the genomic context extends beyond short promoter motifs [62]. A natural 47-bp insertion in *TaSPL6-D* relieves repression of *TaHKT1;5-D* and improves salt tolerance [63]. In bamboo, subgenome expression asymmetry in gibberellin-related genes is associated with variation in UTRs and core promoters [64]. Differences in transcript stability mediated by the 3′UTR can also produce subgenome expression bias in salt-treated rapeseed [65]. The motif combinations, promoter elements and expression patterns in our study describe features that can be compared among members; they do not demonstrate subgenome-specific differences in salt tolerance. Differences in conserved motifs and domains likewise do not establish functional divergence. The 11 members in Fig. 7 were selected by structural type and subgenome, choosing the protein closest to the median length within each stratum. This sampling provides a compact view of family structural variation. Selection did not depend on salt responsiveness or qRT-PCR results, and the representatives have not been assigned validated salt-tolerance functions. Synteny analysis, copy × treatment interaction tests and allele-specific expression analysis are needed to resolve divergence among copies.

4.3.3. Cis-acting elements, association network and priority pair for validation

Cis-acting element analysis identifies specific sites that can be tested experimentally. In wild rice, OsWRKY80 binds a W-box introduced by a 36-bp insertion in the *ST5* promoter and affects regulation, illustrating the need to connect sequence variation with functional evidence [66]. ABRE and W-box core motifs occurred upstream of nearly all evaluable WRKY genes in our study (Fig. 7c). Their widespread occurrence suggests possible sites for

testing hormonal inputs and WRKY-related regulation, but does not demonstrate binding, WRKY autoregulation or direct regulation of *P5CS*/*P5CR*. The two TTGACT motifs upstream of Dl3AG001551 provide coordinates for site-directed mutagenesis; their presence alone does not establish specific regulation. Conversely, the absence of either scanned W-box core motif upstream of Dl14AG001137 does not exclude WRKY regulation. Detection also depends on the length of sequence available. *DlWRKY121* had only a 30-bp usable upstream region, so its zero hits cannot establish the absence of regulatory elements. The analysis matched a fixed panel of sequences without binding prediction or enrichment testing. Coordinate 0 denotes the annotated 5′ gene boundary, not an experimentally determined TSS.

The reference network assembled from merged mappings suggests that some groups of salt-responsive WRKY members are relatively well connected. However, the 110 candidate links in Fig. 8 were projected from 30 reference associations and do not provide independent interaction evidence. Few edges were predicted as physical associations, all had an experimental-channel score of 0, and edge counts declined sharply under stricter thresholds and mapping criteria. Network interpretation therefore depends on homology mapping and the type of evidence used. *DlWRKY057*, *DlWRKY063* and *DlWRKY070*, for example, map to the same rice protein. Their high degree cannot be treated as separate evidence for each *D. latiflorus* gene or used to identify one copy as a functional hub. Experimental studies show how WRKY partners can influence transcription. Apple MdVQ17 and MdVQ37 interact with MdWRKY100 and suppress its activation of *MdAKT1-like* and *MdPER57* [67]. Rice OsGH17 binds the disordered region of OsWRKY1 and affects condensate formation and DNA binding [68]. Apple MdWOX11 interacts with MdWRKY75 and weakens its repression of *MdSAUR15* [69]. These findings show that cofactors can change WRKY transcriptional output, while also demonstrating why protein interaction, DNA binding and transcriptional effects require separate tests. Our network can help select candidate partners for such

749 experiments. It does not assess the proposed regulation of P5CS by WRKY: the reference
750 group containing *DlWRKY004* is isolated, and P5CS was absent from the network. The
751 promoter-regulation hypothesis should therefore not be described as an interaction between
752 WRKY and the P5CS enzyme protein.

753 Some WRKY and P5CS expression correlations weakened after treatment means were
754 subtracted (Section 3.8), suggesting that a shared salt response accounts for part of the
755 original association. None of the within-treatment permutation tests for the 85 candidate pairs
756 remained significant after multiple-testing correction, leaving insufficient evidence for co-
757 variation within treatments. Co-expression was therefore not used to assign regulatory edges.
758 Candidate ranking instead considered gene-structure completeness, the two catalytic domains
759 and W-box core motifs with defined coordinates. On this basis, direct regulation of
760 Dl3AG001551 by *DlWRKY004* is a hypothesis for testing. Establishing a causal relationship
761 will require confirmation of the target, site binding and transcriptional effects, followed by
762 measurements of metabolic output and salt tolerance. The identity and amplification
763 performance of the qRT-PCR target should be confirmed first. Yeast one-hybrid, EMSA or
764 ChIP-qPCR could then test binding of *DlWRKY004* to the two TTGACT sites, while a dual-
765 luciferase assay with mutated sites could test whether the transcriptional effect depends on
766 those sequences. *DlWRKY208* can be examined in parallel. If binding or reporter activity is
767 supported, overexpression or silencing lines, P5CS activity assays and measurements of
768 proline synthesis and degradation could connect regulation with metabolism. In apple,
769 MdSOS3 rescued salt sensitivity in lines with reduced *MdWRKY75* expression, providing an
770 approach for testing dependence between candidate upstream and downstream genes [70].
771 ROS, ion content and growth or survival should also be measured to determine whether the
772 proposed regulation affects salt tolerance in *D. latiflorus*.

5. Conclusions

Responses of *D. latiflorus* to NaCl varied among physiological processes and across salt concentrations. CAT activity reached 2.02 times the control level at low salinity, and the number of candidate DEGs peaked at moderate salinity (4,424). At high salinity, MDA reached 1.95 times the control level while carotenoids declined by 15.8%. Proline increased with salt concentration to 2.70 times the control level at T3, corresponding at the treatment level with expression changes in biosynthetic genes. Transcriptomic enrichment implicated osmotic adjustment, signal transduction and secondary metabolism. Arginine and proline metabolism was enriched in all three salt treatments, with expression changes concentrated in *P5CS* rather than *P5CR*. Among the DEGs, 17 salt-responsive WRKY genes showed up-regulated, persistently down-regulated or mixed expression patterns. Genome-wide analysis identified 488 candidate WRKY models and 245 A1/B1/C1 representative members in the I-like, II-like, III-like and Atypical groups. Conserved motifs centred on WRKYGQK are common in the family, and ABRE and W-box core motifs are common in their upstream regions.

Expression responses, protein completeness and promoter sites identified *DlWRKY004* (Dl1AG000697) and the P5CS candidate Dl3AG001551 as the priority pair for validation, with *DlWRKY208* as an alternative. The two TTGACT-type W-box core motifs upstream of Dl3AG001551 define sites for mutagenesis and binding tests. The reference network based on homology can also guide the selection of WRKY partners. Direct regulation, protein interaction and functional divergence among subgenomes have not yet been established. Confirming target identity and combining binding assays with metabolic measurements and genetic experiments will allow the contributions of these WRKY genes and their downstream targets to salt tolerance in *D. latiflorus* to be tested.

Declarations

Abbreviations

ABA, abscisic acid; ABRE, ABA-responsive element; CAT, catalase; CDS, coding sequence; CPM, counts per million; Ct, threshold cycle; DEG, differentially expressed gene; FDR, false discovery rate; GO, Gene Ontology; GSA, glutamate 5-semialdehyde; KEGG, Kyoto Encyclopedia of Genes and Genomes; MDA, malondialdehyde; P5C, Δ^1-pyrroline-5-carboxylate; P5CR, P5C reductase; P5CS, P5C synthase; PCA, principal component analysis; POD, peroxidase; qRT-PCR, quantitative reverse-transcription PCR; ROS, reactive oxygen species; SD, standard deviation; SOD, superoxide dismutase; TMM, trimmed mean of M-values; TPM, transcripts per million; UFBoot, ultrafast bootstrap.

Ethics approval and consent to participate

Permission to collect *Dendrocalamus latiflorus* Munro from public land in Yunyang Village, Lianhua Town, Tong'an District, Xiamen, Fujian Province, China, was obtained from the authority responsible for managing the land. The plant material was identified as *Dendrocalamus latiflorus* Munro by Yushan Zheng. A living voucher traceable to the original collection is registered under accession no. 350212 and maintained at Fujian Nanjing Yongfeng State-owned Forest Farm, Fujian Province, China. The living material is accessible to researchers upon request.

Consent for publication

All authors have read and approved the final manuscript and agree to its publication.

Availability of data and materials

The raw RNA-seq data have been uploaded to the Genome Sequence Archive (GSA) at the National Genomics Data Center under BioProject PRJCA079155. Other data supporting the findings of this study are available from the corresponding authors upon reasonable request.

Requests should be directed to Yushan Zheng (zys1960@163.com) or Jundong Rong (rongjd@fafu.edu.cn).

Competing Interests

The authors declare that they have no competing interests.

Funding

This research was supported by the National Key Research and Development Program of China (2023YFD2201201) and the Fujian Agriculture and Forestry University Science and Technology Innovation Project (KFB24066).

Authors' contributions

HT drafted and revised the manuscript and contributed to software and methodology. LP contributed to the investigation, formal analysis and data curation. RX, CS, LGC, TH and LYC contributed to the investigation and data curation. JR supervised the work and administered the project. YZ supervised and administered the project and acquired funding. All authors read and approved the final manuscript.

Acknowledgements

Not applicable.

References

1. Wu Y, Yuan J, Shen L, Li Q, Li Z, Cao H, et al. A phosphorylation-regulated NPF transporter determines salt tolerance by mediating chloride uptake in soybean plants. EMBO J. 2025;44:923-946. https://doi.org/10.1038/s44318-024-00357-1.

2. Zhang M, Zhou X, Wang L, Liang X, Liu X, Jiang C. A SnRK2-HAK regulatory module confers natural variation of salt tolerance in maize. Nat Commun. 2025;16:4026. https://doi.org/10.1038/s41467-025-59332-x.

844 3. Li KL, Xue H, Tang RJ, Luan S. A calcium sensor kinase pathway interacts with the TOR
845 complex to balance growth and salt tolerance in Arabidopsis. Plant Cell. 2025;37:koaf103.
846 https://doi.org/10.1093/plcell/koaf103.
847 4. Poitout A, Ugalde JM, Gorgues L, Dongois A, Scholz P, Nacry P, et al. Nanoscale
848 regulation of ROS signaling at the plasma membrane tunes the plant response to osmotic
849 stress. Proc Natl Acad Sci USA. 2026;123:e2529740123.
850 https://doi.org/10.1073/pnas.2529740123.
851 5. Fang H, Gao X, Wu Y, Zhang K, Wu Y, Li J, et al. Unveiling the role of GhP5CS1 in
852 cotton salt stress tolerance: a comprehensive genomic and functional analysis of P5CS genes.
853 Plants. 2025;14:231. https://doi.org/10.3390/plants14020231.
854 6. Dong H, Di Y, Guo Z, Lou S, Ji Z, Wang Z, et al. The CRYPTOCHROME 1a-
855 ELONGATED HYPOCOTYL 5 module regulates blue light-induced salt stress tolerance in
856 tomato. Plant Physiol. 2025;199:kiaf538. https://doi.org/10.1093/plphys/kiaf538.
857 7. Rajappa S, Krishnamurthy P, Huang H, Yu D, Friml J, Xu J, et al. The translocation of a
858 chloride channel from the Golgi to the plasma membrane helps plants adapt to salt stress. Nat
859 Commun. 2024;15:3978. https://doi.org/10.1038/s41467-024-48234-z.
860 8. Peng L, Chao D, Sun X, Li L, Yu J, Li Z, et al. OsWRKY18, a WRKY transcription factor,
861 is involved in rice salt tolerance. Plant Cell Physiol. 2025;66:1169-1183.
862 https://doi.org/10.1093/pcp/pcaf063.
863 9. Zhao J, Zhang S, Yu Z, Gu T, Zhang J, Meng L, et al. The transcription factor MdWRKY9
864 is involved in jasmonic acid-mediated salt stress tolerance in apple. Hortic Res.
865 2025;12:uhaf068. https://doi.org/10.1093/hr/uhaf068.
866 10. Ma Z, Jia Y, Huang W, Wu H, Fang X, Ma Q, et al. ZmWRKY17 negatively regulates
867 salt tolerance through ABA signaling pathway in maize. Acta Physiol Plant. 2025;47:11.
868 https://doi.org/10.1007/s11738-024-03763-4.

11. Liu X, Duan P, Shang C, Li Q, Yang J, Yan J, et al. SlWRKY42 positively promotes proline accumulation by regulating SlP5CS1 to enhance tomato salt stress tolerance. J Integr Agric. 2025. Advance online publication. https://doi.org/10.1016/j.jia.2025.11.007.

12. Zhu C, Lin Z, Liu Y, Li H, Di X, Li T, et al. A bamboo HD-Zip transcription factor PeHDZ72 conferred drought tolerance by promoting sugar and water transport. Plant Cell Environ. 2025;48:310-322. https://doi.org/10.1111/pce.15105.

13. Ye Y, Chang Y, Zhang W, Chu T, Tian H, Deng Y, et al. Identification and functional validation of the PeDHN gene family in moso bamboo. Plants. 2025;14:1520. https://doi.org/10.3390/plants14101520.

14. Liang J, Zhou L, Hu X, Lu J, Wang W, Zhu Q. Functional and expression profiling of DREB genes in Ma bamboo (*Dendrocalamus latiflorus* Munro) reveals their role in abiotic stress adaptation. Plant Physiol Biochem. 2025;228:110203. https://doi.org/10.1016/j.plaphy.2025.110203.

15. Wang N, Cheng Y, Yan Z, Xu J, Zheng J, Wang Y, et al. The DlamiR156-DlaSPL60-DlaP5CS1 cascade directly regulates proline synthesis, conferring drought tolerance in Ma bamboo (*Dendrocalamus latiflorus* Munro). New Phytol. 2026;252:1112-1129. https://doi.org/10.1111/nph.71542.

16. Zheng Y, Yang D, Rong J, Chen L, Zhu Q, He T, et al. Allele-aware chromosome-scale assembly of the allopolyploid genome of hexaploid Ma bamboo (*Dendrocalamus latiflorus* Munro). J Integr Plant Biol. 2022;64:649-670. https://doi.org/10.1111/jipb.13217.

17. Ma PF, Liu YL, Guo C, Jin G, Guo ZH, Mao L, et al. Genome assemblies of 11 bamboo species highlight diversification induced by dynamic subgenome dominance. Nat Genet. 2024;56:710-720. https://doi.org/10.1038/s41588-024-01683-0.

892 18. Wang YJ, Guo C, Zhao L, Mao L, Hu XZ, Yang YZ, et al. Haplotype-resolved nonaploid
893 genome provides insights into in vitro flowering in bamboos. Hortic Res. 2024;11:uhae250.
894 https://doi.org/10.1093/hr/uhae250.
895 19. Du C, Yun Y, Li W, Wu X, Liu X, Li M, et al. A natural variation within duplicated
896 AsWRKY49-D2 drives the subgenomic functional divergence of homeologs in salt response
897 of allohexaploid oats. J Integr Plant Biol. 2026;68:1367-1383.
898 https://doi.org/10.1111/jipb.70171.
899 20. Kim D, Paggi JM, Park C, Bennett C, Salzberg SL. Graph-based genome alignment and
900 genotyping with HISAT2 and HISAT-genotype. Nat Biotechnol. 2019;37:907-915.
901 https://doi.org/10.1038/s41587-019-0201-4.
902 21. Pertea M, Pertea GM, Antonescu CM, Chang TC, Mendell JT, Salzberg SL. StringTie
903 enables improved reconstruction of a transcriptome from RNA-seq reads. Nat Biotechnol.
904 2015;33:290-295. https://doi.org/10.1038/nbt.3122.
905 22. Liao Y, Smyth GK, Shi W. featureCounts: an efficient general purpose program for
906 assigning sequence reads to genomic features. Bioinformatics. 2014;30:923-930.
907 https://doi.org/10.1093/bioinformatics/btt656.
908 23. Li B, Dewey CN. RSEM: accurate transcript quantification from RNA-Seq data with or
909 without a reference genome. BMC Bioinformatics. 2011;12:323.
910 https://doi.org/10.1186/1471-2105-12-323.
911 24. Chen Y, Lun A, Smyth G. From reads to genes to pathways: differential expression
912 analysis of RNA-Seq experiments using Rsubread and the edgeR quasi-likelihood pipeline.
913 F1000Research. 2016;5:1438. https://doi.org/10.12688/f1000research.8987.2.
914 25. KEGG. Proline biosynthesis, glutamate => proline (KEGG module M00015).
915 https://www.kegg.jp/module/M00015. Accessed 23 Oct 2026.

916 26. National Center for Biotechnology Information. Primer-BLAST: a tool for finding
917 specific primers. https://www.ncbi.nlm.nih.gov/tools/primer-blast/. Accessed 1 Nov 2026.
918 27. Livak KJ, Schmittgen TD. Analysis of relative gene expression data using real-time
919 quantitative PCR and the $2^{-\Delta\Delta C(T)}$ method. Methods. 2001;25:402-408.
920 https://doi.org/10.1006/meth.2001.1262.
921 28. Bustin SA, Ruijter JM, van den Hoff MJB, Kubista M, Pfaffl MW, Shipley GL, et al.
922 MIQE 2.0: revision of the minimum information for publication of quantitative real-time PCR
923 experiments guidelines. Clin Chem. 2025;71:634-651.
924 https://doi.org/10.1093/clinchem/hvaf043.
925 29. Eddy SR. Accelerated profile HMM searches. PLoS Comput Biol. 2011;7:e1002195.
926 https://doi.org/10.1371/journal.pcbi.1002195.
927 30. Katoh K, Standley DM. MAFFT multiple sequence alignment software version 7:
928 improvements in performance and usability. Mol Biol Evol. 2013;30:772-780.
929 https://doi.org/10.1093/molbev/mst010.
930 31. Minh BQ, Schmidt HA, Chernomor O, Schrempf D, Woodhams MD, von Haeseler A, et
931 al. IQ-TREE 2: new models and efficient methods for phylogenetic inference in the genomic
932 era. Mol Biol Evol. 2020;37:1530-1534. https://doi.org/10.1093/molbev/msaa015.
933 32. Bailey TL, Johnson J, Grant CE, Noble WS. The MEME Suite. Nucleic Acids Res.
934 2015;43:W39-W49. https://doi.org/10.1093/nar/gkv416.
935 33. Lescot M, Déhais P, Thijs G, Marchal K, Moreau Y, Van de Peer Y, et al. PlantCARE, a
936 database of plant cis-acting regulatory elements and a portal to tools for in silico analysis of
937 promoter sequences. Nucleic Acids Res. 2002;30:325-327.
938 https://doi.org/10.1093/nar/30.1.325.

939 34. Szklarczyk D, Nastou K, Koutrouli M, Kirsch R, Mehryary F, Hachilif R, et al. The
940 STRING database in 2025: protein networks with directionality of regulation. Nucleic Acids
941 Res. 2025;53:D730-D737. https://doi.org/10.1093/nar/gkae1113.
942 35. Zhuang Y, Zhang Y, Shi H, Pang Y, Feng X, Fan W, et al. CALMODULIN-BINDING
943 RECEPTOR-LIKE CYTOPLASMIC KINASE 3 regulates salt tolerance through
944 CATALASE 2 in Arabidopsis. Plant Physiol. 2025;197:kiae669.
945 https://doi.org/10.1093/plphys/kiae669.
946 36. Liu X, Gao L, Yun Q, Wang W, Liu X, Tang W, et al. Protein tyrosine phosphatase IBR5
947 positively affects salt stress response by modulating CAT2 activity. Plant Sci.
948 2025;359:112615. https://doi.org/10.1016/j.plantsci.2025.112615.
949 37. Cheng X, Li J, Chen G, Zhou Z, Zhu T, Sun Y, et al. The BAHD acyltransferase STBR1
950 confers both saline-alkali tolerance and blast resistance by stabilizing the non-canonical
951 catalase CATA to promote H_2O_2 scavenging in rice. Plant Commun. 2026;7:101611.
952 https://doi.org/10.1016/j.xplc.2025.101611.
953 38. Modareszadeh M, Bahmani R, Kim D, Hwang S. Molecular mechanisms of CAX3
954 involved in salt tolerance in Arabidopsis. Plant Physiol Biochem. 2025;223:109902.
955 https://doi.org/10.1016/j.plaphy.2025.109902.
956 39. Liang W, Zhang Z, Yao N, Wang B, Yu W, Zhu Q, et al. Glycolysis and signal
957 transduction participate in Lycium barbarum in response to NaCl stress through protein
958 phosphorylation. BMC Plant Biol. 2025;25:405. https://doi.org/10.1186/s12870-025-06402-3.
959 40. Wang Y, Wu F, Zou R, Xu M, Shan H, Cheng B, et al. The maize sugar transporters
960 ZmSWEET15a and ZmSWEET15b positively regulate salt tolerance in plants. Plant Physiol
961 Biochem. 2024;213:108845. https://doi.org/10.1016/j.plaphy.2024.108845.

962 41. Abuslima E, Kanbar A, Ismail A, Raorane ML, Eiche E, El-Sharkawy I, et al. Salt stress-
963 induced remodeling of sugar transport: a role for promoter alleles of SWEET13. Sci Rep.
964 2025;15:7580. https://doi.org/10.1038/s41598-025-90432-2.
965 42. Su L, Lv A, Wen W, Fan N, You X, Gao L, et al. MsMYB206-MsMYB450-MsHY5
966 complex regulates alfalfa tolerance to salt stress via regulating flavonoid biosynthesis during
967 the day and night cycles. Plant J. 2025;121:e17216. https://doi.org/10.1111/tpj.17216.
968 43. Song Y, Tang H, Zhang Z, Sun X, Ding X, Guo X, et al. A novel MsEOBI-MsPAL1
969 module enhances salinity stress tolerance, floral scent emission and seed yield in alfalfa. Plant
970 Cell Environ. 2025;48:907-922. https://doi.org/10.1111/pce.15183.
971 44. Fu C, Fu Q, Wang S, Wu F, Jiang N, Zhou R, et al. Genome-wide analysis of fatty acid
972 desaturase genes in moso bamboo (Phyllostachys edulis) reveal their important roles in
973 abiotic stresses responses. BMC Genomics. 2024;25:1138. https://doi.org/10.1186/s12864-
974 024-11065-9.
975 45. Nicolas-Espinosa J, Guarnizo AL, Carvajal M, Yepes-Molina L. Whole-plant
976 spatiotemporal responses to salinity reveal osmotic and ionic drivers of salt tolerance in
977 broccoli. BMC Plant Biol. 2026;26:1430. https://doi.org/10.1186/s12870-026-09390-0.
978 46. Chen X, Han H, Cong Y, Li X, Zhang W, Cui J, et al. Ascorbic acid improves tomato salt
979 tolerance by regulating ion homeostasis and proline synthesis. Plants. 2024;13:1672.
980 https://doi.org/10.3390/plants13121672.
981 47. Yan L, Lu M, Riaz M, Tong K, Yu H, Gao G, et al. Exogenous proline enhances salt
982 acclimation in soybean seedlings: modifying physicochemical properties and controlling
983 proline metabolism through the ornithine-glutamate dual pathway. Ecotoxicol Environ Saf.
984 2025;294:118012. https://doi.org/10.1016/j.ecoenv.2025.118012.

985 48. Ma Z, Zhu X, Min Y, Zhao D, Zhang X, Yan H, et al. Mutation of ZmWRKY87 increases
986 maize salt sensitivity by regulating ZmPP2C4 expression. Plant Physiol Biochem.
987 2025;229:110388. https://doi.org/10.1016/j.plaphy.2025.110388.
988 49. Cai R, Yan H, Zhu X, Fang X, Zhao D, Zhang X, et al. ZmWRKY107 modulates salt
989 tolerance in maize plants by regulating ZmPOD52 expression. Planta. 2025;262:49.
990 https://doi.org/10.1007/s00425-025-04777-z.
991 50. Zhou X, Sun Z, Huang Y, He D, Lu L, Wei M, et al. WRKY45 positively regulates
992 salinity and osmotic stress responses in Arabidopsis. Plant Physiol Biochem.
993 2025;219:109408. https://doi.org/10.1016/j.plaphy.2024.109408.
994 51. Wang H, Zheng Y, Wang M, Liu W, Li Y, Xiao D, et al. BcWRKY25-BcWRKY33A-
995 BcLRP1/BcCOW1 module promotes root development for improved salt tolerance in bok
996 choy. Hortic Res. 2025;12:uhae280. https://doi.org/10.1093/hr/uhae280.
997 52. Zhang Z, Tang H, Guo X, Zheng Y, Wang L, Li T, et al. A novel alfalfa MsWRKY75
998 transcription factor negatively regulates seed germination via an abscisic acid-dependent
999 pathway under salinity stress. Plant Cell Physiol. 2025;66:1868-1877.
1000 https://doi.org/10.1093/pcp/pcaf119.
1001 53. Jia S, Wang C, Sun W, Yan X, Wang W, Xu B, et al. OsWRKY12 negatively regulates
1002 the drought-stress tolerance and secondary cell wall biosynthesis by targeting different
1003 downstream transcription factor genes in rice. Plant Physiol Biochem. 2024;212:108794.
1004 https://doi.org/10.1016/j.plaphy.2024.108794.
1005 54. Yu Y, Bu Y, Song T, Wang X, Zhang D, Zhang S, et al. TaWRKY33 positively regulates
1006 TaERF1-A, thereby activating TaP5CS2-mediated proline biosynthesis, which enhances
1007 drought tolerance in wheat (Triticum aestivum L.). Plant Cell Environ. 2026;49:6487-6505.
1008 https://doi.org/10.1111/pce.70642.

55. Liu X, Shang C, Duan P, Yang J, Wang J, Sui D, et al. The SlWRKY42-SlMYC2 module synergistically enhances tomato saline-alkali tolerance by activating the jasmonic acid signaling and spermidine biosynthesis pathway. J Integr Plant Biol. 2025;67:1254-1273. https://doi.org/10.1111/jipb.13839.

56. Shang C, Liu X, Chen G, Zheng H, Khan A, Li G, et al. SlWRKY80-mediated jasmonic acid pathway positively regulates tomato resistance to saline-alkali stress by enhancing spermidine content and stabilizing Na^+/K^+ homeostasis. Hortic Res. 2024;11:uhae028. https://doi.org/10.1093/hr/uhae028.

57. Gu L, Chen X, Hou Y, Cao Y, Wang H, Zhu B, et al. ZmWRKY30 modulates drought tolerance in maize by influencing myo-inositol and reactive oxygen species homeostasis. Physiol Plant. 2024;176:e14423. https://doi.org/10.1111/ppl.14423.

58. Luan Y, Chen Z, Fang Z, Meng J, Tao J, Zhao D. PoWRKY69-PoVQ11 module positively regulates drought tolerance by accumulating fructose in Paeonia ostii. Plant J. 2024;119:1782-1799. https://doi.org/10.1111/tpj.16884.

59. Wang K, Huang S, Li X, Ma J, Li Y, Kong S, et al. Evolutionary analysis of CBFs/DREB1s in temperate and tropical woody bamboos and functional study of PeDREB1A3 under cold and drought stress. Plant Physiol Biochem. 2025;219:109392. https://doi.org/10.1016/j.plaphy.2024.109392.

60. Zhou B, Lv M, Yan W, Luo X, Yao W, Lin S. Genomic expansion and subgenome expression divergence of sugar transporters during polyploid evolution of bamboos. Biology. 2026;15:1614. https://doi.org/10.3390/biology15181614.

61. Wang X, Liu Y, Zhao P, Hou W, Cheng M, Shi X, et al. HebQTLs reveal intra-subgenome regulation inducing unbalanced expression and function among bread wheat homoeologs. Genome Biol. 2025;26:218. https://doi.org/10.1186/s13059-025-03694-4.

62. Jia J, Deng P, Li T, Wang K, Gao L, Zhao G, et al. Transposable elements drive the subgenomic divergence of homoeologous genes to shape wheat domestication and improvement. Plant Commun. 2025;6:101341. https://doi.org/10.1016/j.xplc.2025.101341.

63. Wang M, Cheng J, Wu J, Chen J, Liu D, Wang C, et al. Variation in TaSPL6-D confers salinity tolerance in bread wheat by activating TaHKT1;5-D while preserving yield-related traits. Nat Genet. 2024;56:1257-1269. https://doi.org/10.1038/s41588-024-01762-2.

64. Mao L, Guo C, Niu LZ, Wang YJ, Jin G, Yang YZ, et al. Subgenome asymmetry of gibberellins-related genes plays important roles in regulating rapid growth of bamboos. Plant Divers. 2025;47:68-81. https://doi.org/10.1016/j.pld.2024.10.004.

65. Xu P, Wang Y, Wu Y, Huang S, Yu X. Multi-layered RNA decay mechanisms underlie subgenome-biased homoeologous mRNA stability in salt-stressed allopolyploid plants. Plant J. 2026;127:e71015. https://doi.org/10.1111/tpj.71015.

66. Xing M, Huang J, Yuan Q, Yang Z, Wang Y, Zhao M, et al. A rare allele of ST5 from wild rice enhances salt tolerance in rice. Adv Sci. 2026;13:e16159. https://doi.org/10.1002/advs.202516159.

67. Duan D, Yi R, Shi M, Zhou J, Dong Q, Mao K, et al. The MdVQ17/MdVQ37-MdWRKY100 module coordinates apple salt tolerance by modulating Na^+/K^+ homeostasis and reactive oxygen species scavenging. Plant Physiol. 2025;199:kiaf434. https://doi.org/10.1093/plphys/kiaf434.

68. Wang TJ, Huang S, Tian X, Zhou D, Xing J, Liu W, et al. A β-1,3-glucanase antagonizes a phase-separating WRKY repressor to confer saline-alkaline tolerance in rice. New Phytol. 2026;251:3313-3331. https://doi.org/10.1111/nph.71368.

69. Zuo X, Zhang X, Fan L, Wang Y, Foster T, Liu X, et al. MdWRKY75 interacts with MdWOX11 to modulate root growth under salt stress in apple. Plant J. 2026;125:e70696. https://doi.org/10.1111/tpj.70696.

70. Zhang Z, Wei J, Wei Y, Yan M, Guo J, Jiang X, et al. The MdERF1B-MdWRKY75-MdSOS3 module confers salt tolerance by regulating sodium-potassium homoeostasis in apple. Plant Cell Environ. 2026;49:5647-5663. https://doi.org/10.1111/pce.70568.

Supplementary Files

This is a list of supplementary files associated with this preprint. Click to download.

- Additionalfile1.xlsx